11-18-2019

Structural analysis of allosteric regulation of the regulatory GAF domains of cone photoreceptor phosphodiesterase-6 (PDE6) by cGMP and the inhibitory γ-subunit

Richa Gupta
University of New Hampshire, Durham

Yong Liu
University of North Carolina at Chapel Hill

Huanchen Wang
Signal Transduction Laboratory, NIEHS/NIH

Christopher T. Nordyke
University of New Hampshire, Durham

Ryan Z. Puterbaugh
University of New Hampshire, Durham

See next page for additional authors

Structural analysis of allosteric regulation of the regulatory GAF domains of cone photoreceptor phosphodiesterase-6 (PDE6) by cGMP and the inhibitory γ-subunit

Richa Gupta[a], Yong Liu[b], Huanchen Wang[c], Christopher T. Nordyke[a], Ryan Z. Puterbaugh[a], Krisztina Varga[a], Feixia Chu[a], Hengming Ke[d], Harish Vashisth[b], and Rick H. Cote[a]

[a]Department of Molecular, Cellular and Biomedical Sciences, University of New Hampshire, 46 College Rd., Durham, NH 03824 USA.

[b]Department of Chemical Engineering, University of New Hampshire, 33 Academic Way, Durham, NH 03824 USA.

[c]Signal Transduction Laboratory, NIEHS/NIH, 111 T.W. Alexander Drive, Research Triangle Park, NC, 27709, USA

[d]Department of Biochemistry and Biophysics and Lineberger Comprehensive Cancer Center, The University of North Carolina at Chapel Hill, Chapel Hill, North Carolina 27599 USA

To whom correspondence should be addressed: Rick H. Cote, Department of Molecular, Cellular and Biomedical Sciences, University of New Hampshire, 46 College Rd., Durham, NH 03824 USA; +1 603-862-2458 (p); rick.cote@unh.edu

Keywords: phosphodiesterase, PDE6, allosteric regulation, structural biology, x-ray crystallography, nuclear magnetic resonance spectroscopy, chemical cross-linking, mass spectrometry, integrative structural modeling, visual transduction, photoreceptor**,** molecular dynamics simulations.

This work has not been peer-reviewed.

The authors declare no financial or intellectual competing interests.

Abstract

Regulation of photoreceptor phosphodiesterase (PDE6) activity is responsible for the speed, sensitivity, and recovery of the photoresponse during visual signaling in vertebrate photoreceptor cells. It is hypothesized that the physiological differences in the light responsiveness of rods and cones may result in part from differences in the structure and regulation of the distinct isoforms of rod and cone PDE6. Although rod and cone PDE6 catalytic subunits share a similar domain organization consisting of tandem GAF domains (GAFa and GAFb) and a catalytic domain, cone PDE6 is a homodimer whereas the rod PDE6 catalytic dimer is composed of two homologous catalytic subunits. Here we provide the x-ray crystal structure of cone GAFab regulatory domain solved at 3.3 Å resolution in conjunction with chemical cross-linking and mass spectrometric analysis of conformational changes to GAFab induced upon binding of cGMP and the PDE6 inhibitory γ-subunit (Pγ). Ligand-induced changes in cross-linked residues implicate the α4-helix of GAFa (close to the cGMP binding site) and the β1/β2 loop of GAFb as key motifs that have been previously proposed to communicate with the catalytic domains of PDE6. Molecular dynamics (MD) simulations of cone GAFab revealed asymmetry in the two GAFab subunits forming the homodimer and allosteric perturbations on cGMP binding. Cross-linking of Pγ to GAFab in conjunction with solution NMR spectroscopy of isotopically labeled Pγ identified the central polycationic region of Pγ interacting with the GAFb domain. These results provide a mechanistic basis for developing allosteric activators of PDE6 with therapeutic implications for halting the progression of certain retinal degenerative diseases.

Introduction

The vertebrate retina contains two types of photoreceptors, rods and cones, that differ in their responsiveness to light. For example, while rods are hundred times more light-sensitive than cones, cone electrical responses are faster during both the excitation and recovery phases {Korenbrot, 2012 #7097;Ingram, 2016 #7800}. The first step in vision involves photoisomerization of the visual pigment rhodopsin which activates a G-protein mediated signaling cascade leading to activation of a cGMP-specific phosphodiesterase (PDE6) in the outer segment of rod and cone cells. This results in lowering of cGMP levels and closure of cGMP-gated ion channel leading to membrane hyperpolarization {Arshavsky, 2012 #7055}. Rod and cone photoreceptors express homologues of all of the phototransduction components mentioned above {Korenbrot, 2012 #7097}. Whereas cone PDE6 (gene name: PDE6C) consists of two identical catalytic subunits to which two cone-specific inhibitory γ-subunits (gene name: PDE6H) bind, rod PDE6 is a catalytic heterodimer (gene names: PDE6A and PDE6B) whose activity is regulated by two rod-specific inhibitory γ-subunits (gene name: PDE6G).

In mammals, there are eleven Class I PDE families that share a highly conserved catalytic domain whose catalytic activity is regulated by the N-terminal regulatory domain {Conti, 2007 #6660;Francis,

2011 #6969}. Of the eleven PDE families, five (PDE2, PDE5, PDE6, PDE10, and PDE11) contain two tandem regulatory GAF domains (GAFa and GAFb), so named for the identification of this protein domain in c**G**MP-binding phosphodiesterases, cyanobacterial **A**denylyl cyclases and transcription factor **F**hlA {Heikaus, 2009 #6958}. Binding of cGMP to the GAFa domain of PDE5 results in allosteric stimulation of catalytic activity {Zoraghi, 2004 #5442;Wang, 2010 #6963;Biswas, 2011 #7075}. PDE6 GAF domains are believed to serve multiple functions: (a) enhance dimerization of the catalytic subunits; (b) contribute to the high overall binding affinity of Pγ; and (c) communicate allosterically between the GAF and catalytic domains {Cote, 2006 #5841}.

There is substantial biochemical evidence for allosteric regulation of rod PDE6 by its GAF domains. For example, binding of cGMP to the GAFa domain enhances the binding of Pγ to the rod PDE6 catalytic heterodimer, whereas binding of Pγ increases the affinity of cGMP to the noncatalytic cGMP binding site in GAFa {Muradov, #4864;Zhang, 2008 #6869}. In addition, binding of PDE5/6 inhibitor compounds to the enzyme active site decreases the rate of dissociation of cGMP from the GAFa domain {Zhang, 2008 #6869}. However, the structural and functional basis for this reciprocal allosteric regulation of PDE6 by binding of cGMP and Pγ is poorly understood.

The x-ray crystal structures of several GAF-containing PDEs have been reported, including nearly full-length unliganded PDE2 {Pandit, 2009 #6985}, cGMP bound GAFab of PDE2 {Martinez, 2002 #7575}, the unliganded GAFab dimer of PDE5 {Wang, 2010 #6963}, and the isolated GAFa domain of cone PDE6C with bound cGMP {Martinez, 2008 #6847}. More recently, a cryo-EM structure of rod PDE6 with cGMP bound to the GAFa domains has been determined that provides hypotheses about the allosteric communication that may occur between the regulatory and catalytic domains {Gulati, 2019 #7980}. However, experimental evidence is lacking on the structural changes that are induced by binding of cGMP or Pγ to the regulatory GAF domains.

In this study, we report 3.3 Å x-ray crystal structure of the unliganded GAFab of PDE6C where its GAFa domain has close structural similarity to rod PDE6 and PDE5 GAFab domains but the PDE6C GAFb domain exhibiting significant structural differences. We hypothesized that binding of cGMP and Pγ induces discrete conformational changes that originate in the regulatory GAF domains and communicated to the catalytic domains, thereby providing a mode of allosteric regulation of the active lifetime of PDE6. To test this, chemical cross-linking and mass spectrometry analysis (CXMS) were used to characterize the conformational changes that occur upon binding of Pγ or/and cGMP to GAFab. Integrative structural modeling of the cross-linked peptides observed in the four possible liganded states (apo, cGMP bound, Pγ bound, and cGMP and Pγ bound) revealed discrete structural changes that occur in both GAFa and GAFb domains upon binding of cGMP or/and Pγ to GAFab. MD simulations of the cross-link refined apo state structure and the cGMP-bound structure substantiated our hypothesis that cGMP

binding induces conformational changes that are allosterically communicated to the GAFb domain, and also supported the idea that the homodimer has intrinsic structural asymmetry. NMR spectroscopy analysis of isotopically-labeled Pγ in the absence or presence of GAFab identified the central polycationic region of Pγ as the primary site of interaction with the GAFb domain of PDE6C. This study provides the most comprehensive analysis of allosterically-induced conformational changes in cone photoreceptor PDE6 that likely contributes to determining the basal activity and the activated lifetime of PDE6 during visual transduction in rod and cone photoreceptors.

Results

X-ray structure of the cone PDE6 regulatory GAF domains.

Because of the inability to heterologously express full-length cone PDE6 catalytic subunits in sufficient quantities for structural studies {Gopalakrishna, 2016 #7647}, we relied on previous success with expression of PDE5 GAFab {Wang, 2010 #6963} and the isolated GAFa domain of chicken cone PDE6C {Martinez, 2008 #6847} to construct expression vectors for bacterial expression and purification of residues 42-458 of chicken cone PDE6C containing a 6His tag (Fig. S1A). We also expressed and purified the corresponding chicken cone Pγ subunit consisting of its first 58 residues. Purified recombinant GAFab was judged to be properly folded, based on its apparent MW observed by gel filtration as well as its ability to bind cGMP to the GAFa domain with a K_D value (20 nM) similar to values reported previously [Fig. S1B; {Huang, 2004 #5662}].

Purified PDE6C GAFab was then crystallized, and its structure determined from crystals in the space group of $P6_5$ with cell dimensions of a = b = 148.5, and c = 93.7 Å (Table 1). The structure was solved by using the PDE5 GAFab structure (Wang et al., 2010) as the initial model, and refined to R-factor of 0.207 for 16489 reflections at 3.2 -50 Å resolution (Table 1). Residues 48-451 of the primary sequence of PDE6C were traceable, except for residues Lys286 to Thr309 (Fig. 2A, *arrows*). Fig. S2 provides domain boundaries and secondary structure elements for the PDE6C GAFab structure.

The PDE6 GAFab molecule is a homodimeric structure (Fig. 2A) that has the same fold as the homodimeric GAFab domains of PDE2 (Pandit, 2009) and PDE5 (Wang et al., 2010), as well as with the heterodimeric rod PDE6 [Fig. 2B; (Irwin et al., 2019){Gulati, 2019 #7980}. The two subunits of the cone GAFab dimer overall exhibit symmetry (RMSF = 0.74 Å; Fig. S1C).

The structural superposition of the PDE6C GAFa (residues 74-225) over its cGMP complex from (Martinez et al., 2008) revealed an average shift of 0.6 Å for the Cα atoms, suggesting that cGMP binding does not induce dramatic conformational changes within the GAFa domain (Fig. 2C). The largest movement among the cGMP binding residues (Phe99, Leu115, Asn116, Phe136, Ser165, and Thr172,

Figs. 2C and 2D) is 1.1 Å for the Cα Asn116 whose side chain forms a hydrogen bond with the base nitrogen of cGMP.

A comparison of the rod {Irwin, 2019 #8185} and cone GAFab structures (Fig. 2A) reveals greater differences in the GAFb domains compared with more limited structural differences predicted for the GAFa domains (Fig. S3). Excluding the N-terminal and C-terminal regions, the average RMSD for GAFa was approximately 2-fold lower than for GAFb (mean RMSD values of 3.6 Å and 6.3 Å, respectively). These structural differences may reflect underlying functional differences in the allosteric regulatory mechanisms of rod and cone PDE6, especially in the GAFb domain where a previous study suggesting that the β1/β2 loop of GAFb may serve as a relay for signaling cGMP occupancy from the GAFa binding site to the active site in the catalytic domain {Gulati, 2019 #7980}.

Solution structure of the unliganded state of GAFab determined by chemical cross-linking and mass spectrometry

To investigate the allosteric regulation of the PDE6C GAFab regulatory domain, we first carried out chemical cross-linking coupled with liquid chromatography/mass spectrometry (XL-MS) to evaluate the structure of GAFab in solution and to create a structural model for the missing residues that were not resolved in the crystal structure. Fig. 3A shows a typical cross-linking experiment using BS3 that shows the appearance of gel-shifted bands corresponding to the cross-linked GAFab dimer. We also conducted cross-linking experiments in the presence of cGMP and/or Pγ1-58 (described below). The gel bands corresponding to the GAFab dimer (~100 kDa) were excised, proteolyzed, and analyzed by MS. Cross-linked peptides identified for the GAFab apo state were used as spatial restraints for integrative structural modeling using the crystal structure as the template.

Fig. 3B demonstrates that the solution structure of the apo state of GAFab, refined by spatial restraints imposed by more than 40 cross-links, was very similar to the x-ray structure in Fig. 2A. In particular, most of the α-helical and β-strand secondary structural features of the cross-linking-based structural model superimpose well with the crystal structure. Fig. S4 shows an RMSD plot as a function of amino acid residue number and includes the location of the cross-linking sites that were used in structural modeling of the GAFab solution structure in its apo state. Structural alignment of the GAFa domains of the apo and crystal structure (Fig. 3C) reveal that the spatial restraints imposed by the cross-linking data result in significant differences in the solution structure in the α4 helix (near the opening to the cGMP binding site), and the β4 strand and adjoining loop region (residues 199 to 205). The GAFb domain of the solution structure also closely superimposes on the crystal structure (Fig. 3D), with the cross-linking results allowing us to generate a structural model for the β1/β2 loop (residues 288 to 310) that was missing in the crystal structure.

Structural differences of GAFab complexed with cGMP and/or Pγ revealed by chemical cross-linking/MS analysis

Fig. 4 compares the cross-link-refined structures for the apo GAFab with the cGMP-bound, Pγ-bound, and cGMP and Pγ bound states. RMSD plots for the various liganded states (Fig. S5) show that binding of either cGMP or Pγ1-58 induces perturbations in the structures that are primarily localized to the GAFb β1/β2 loop region and the GAFa α4/β4 region. Both structural elements have been proposed to participate in allosteric communication from the GAF domains to the catalytic domains of PDE6 {Gulati, 2019 #7980;Irwin, 2019 #8185}. 24 cross-links obtained from XL-MS analysis of the cGMP bound state of GAFab were used to refine apo structure to create a model for cGMP-bound GAFab. Comparison of cGMP bound versus the apo GAFab reveals a small conformational change in the α4 region of GAFa, consistent with previous studies.{Huang, 2004 #5662}. A conformational change in the GAFb β1/β2 loop that places it closer to the cGMP binding site in GAFa was supported by three cross-links (residues 169-308, 308-289 and 288-305; Fig 4B). When comparing the cGMP-bound GAFa structure (PDBID: 3DBA) with our results, the α3,α4 and β strands forming the cGMP pocket in GAFa have similar conformations.

We identified 54 cross-links that were used to model the structure of GAFab bound to Pγ, while 59 cross-links were found for the cGMP/Pγ bound form of GAFab. In contrast to the apo GAFab or cGMP-bound states of GAFab, Pγ-bound GAFab showed downward displacement of the GAFb β1/β2 loop, similar to that reported for rod PDE6 {Gulati, 2019 #7980}{Irwin, 2019 #8185}. Binding of Pγ to GAFab also resulted in displacement of GAFa domain particularly α4 region toward GAFb as compared to Apo GAFab (Fig 4A). Conformational changes observed in both Pγ and cGMP bound GAFab are similar to those found in only Pγ bound state of GAFab (Fig 4C).

Molecular dynamics (MD) simulations of unliganded and cGMP-bound GAFab reveal subunit asymmetry and allosteric communication

To evaluate the conformational dynamics and allosteric coupling within the two subunits of the PDE6 homodimer, we carried out three independent long time-scale MD simulations (see Methods and Table S1) of the PDE6 crystal structure as well as of the refined (based on cross-linking data) structural models of the PDE6 in the apo and cGMP-liganded states. For all simulations based on each of these PDE6 structures, we computed various conformational metrics (root mean squared deviation/fluctuation, RMSD/F; buried surface area, BSA; inter-domain center-of-mass distances, dynamic residue-residue cross correlation, DCC) that provide details on dynamics spanning individual residues to subdomains (GAFa/GAFb). The RMSD analysis reports on the flexibility of individual subdomains, RMSF reports on the flexibility of each amino acid residue, DCC analysis reports on correlated motions, while inter-domain

center-of-mass distances and BSA report on the relative movements and buried surface areas between subdomains.

Analysis of the crystal structure—assessment of the stability of the subdomain structural fold: In Fig. S6, we report data on conformational metrics based on simulations of the crystal structure of PDE6 homodimer. The results based on RMSF and RMSD data (panels B and C in Fig. S6) show that the GAFa and LH1 subdomains in each subunit (Fig. S6A) are least flexible, while GAFb subdomains show bimodal RMSD distributions highlighting two distinct conformational states. The overall RMSD values for all subdomains range between 0-6 Å except those of the LH2 subdomains which range between 0-10 Å (with mean values ~5 Å). The higher flexibility of the LH2 domain is due to their location at the free termini of subunits. We also observed that the BSA between GAFa subdomains (~70-280 $Å^2$) is significantly higher than the BSA between GAFb subdomains (~0-120 $Å^2$). We observed the highest BSA between the LH1 motifs (~1100-14000 $Å^2$) followed by BSA between the C-terminal (~500-1100 $Å^2$) and N-terminal helices (~300-800 $Å^2$), respectively. Collectively, these data indicate that the overall subdomain folds resolved in the crystal structure as well as interfacial contact areas between subdomains are stably maintained in solutions states explored by MD simulations.

Analysis of the apo and cGMP-liganded states of PDE6—subunit asymmetry and allosteric communication. In Fig. 5, we report ΔRMSF values comparing each chain of the homodimer in the apo and cGMP-liganded states. A value of ΔRMSF = 0 (or a very small difference) for each residue will indicate that the homodimer is dynamically evolving in a symmetric way with no major differences between individual chains and their subdomains. However, we observed that both GAFa and GAFb domains from each chain show a finite and non-negligible difference in flexibility per residue with GAFb domains showing more pronounced differences. This highlights asymmetric conformational evolution of the PDE6 homodimer both in the apo state and in the cGMP bound state.

In Figs. S7 and S8, we report conformational metrics for the apo and cGMP-liganded states. These data highlight that the distributions of RMSD for GAFa subdomains are unimodal in the apo state, but bimodal in the cGMP bound state indicating a lower population of a moderately more flexible state on binding of cGMP. This trend is further captured in BSA distributions where more buried surface between GAFa domains is observed in the cGMP bound state of the homodimer in comparison to the apo-state suggesting that the GAFa subdomains move closer to each other on cGMP binding. For GAFb subdomains, we do not observe any major differences as the distributions of RMSD in both apo and cGMP bound states are bimodal. Similarly, for other structural motifs, the RMSD distributions do not highlight any major differences in flexibility, but BSA distributions show that the BSA between the helical motifs at the N- and C-terminus significantly increased on cGMP binding. This observation

highlights allosteric perturbations on cGMP binding, mostly stabilizing interfaces between the terminal motifs. We surmise that the C-terminal helices moving closer could alter the conformation of catalytic domains thereby highlighting the role of cGMP in initiating allosteric communication. Our residue-residue DCC analysis (Fig. 6) further showed signatures of asymmetry and allostery within the individual subunits of the PDE6 homodimer. For example, the LH2 motif showed increased correlation with residues in the GAFb subdomain of chain B on cGMP binding, while the same motif showed increased correlation with the GAFa subdomain in chain A on cGMP binding. We also observed that on cGMP binding, the LH1 motifs became more correlated with the GAFa subdomains in respective chains of the homodimer, while simultaneously several loops in GAFa/GAFb subdomains became less correlated within the respective chains. Collectively, MD simulation analyses provided evidence for the stability of the solution state fold of the PDE6 conformation observed in the crystal structure, or asymmetry in the dynamics of each chain, and allosteric perturbations on cGMP binding.

Binding of the central region of Pγ to the GAFb domain

Our XL-MS analysis identified 18 inter-subunit cross-links for the Pγ bound state of GAFab and 17 inter-subunit cross-links for GAFab bound to both Pγ and cGMP. These cross-links permitted integrative structural modeling with the Integrated Modeling Platform to "dock" residues 23 to 50 of Pγ [using bovine rod Pγ as template {Irwin, 2019 #8185}]. Due to the fact that cone PDE6C is a homodimer, it was not possible to assign inter-molecular cross-linked peptides of Pγ and GAFab to one of the two subunits. For this reason, we applied all of the observed Pγ-GAFab cross-links to both subunits. Residues 23-50 of Pγ were identified as interacting with the GAFb domains, consistent with the localization of the homologous region of rod Pγ with the rod GAFb domains {Irwin, 2019 #8185}. Pγ docked similarly in both conditions Pγ_GAFab and Pγ_cGMP bound GAFab, and Fig7 shows the Pγ 23-50 docked in Pγ_GAFab state. The absence of reactive lysine residues in the first 23 amino acids of the cone Pγ sequence prevented us from obtaining cross-linking results for the N-terminal region of Pγ.

Characterization of cone Pγ1-58 and its binding to GAFab by solution NMR spectroscopy.

Solution NMR spectroscopy was utilized to further characterize Pγ and its interactions with GAFab. Isotopically enriched Pγ (^{13}C, ^{15}N) was expressed in *E. coli,* purified, and standard 2-dimensional (2D) and 3-dimensional (3D) solution NMR experiments were performed for Pγ backbone and side chain assignments. The narrow dispersion of backbone ^{1}H chemical shifts between 7.5 and 0.9 ppm in the2D ^{1}H-^{15}N HSQC spectrum is indicative of the intrinsically disordered nature of Pγ. In contrast, well-ordered protein spectra are typically characterized by a wider dispersion of backbone ^{1}H resonances well beyond

the 1.5 ppm range of intrinsically disordered proteins. Based on 3D HNCA, HNCACB, and HNCO spectra, 46 of the 58 Pγ resonances were assigned (Fig 8A). The only residues that could not be assigned were the 9 prolines and the first 3 amino acids of the sequence.

To probe the binding interface of Pγ, we mixed the chicken cone Pγ fragment (isotopically enriched) with the regulatory GAFab domain (unlabeled, natural abundance). The addition of GAFab induced significant changes in the Pγ ^{1}H-^{15}N HSQC spectrum (Fig 8B). The Pγ residues that make contact with GAFab are expected to exhibit the greatest chemical shift perturbations and NMR signal broadening resulting in signal attenuation. The most significant effects were observed for the F28-S38 region, where the peaks were barely detectable, very close to the baseline. Smaller attenuation and shifts were observed for neighboring residues (e.g. T20, G24, K27, and K42), which suggests that although these residues may not be directly interacting with GAFab, they are in close proximity to the binding interface and are affected by indirect effects. The N-terminal residues (N4-D13) of Pγ were the least affected by the binding, as inferred not only from the lack of chemical shift perturbations but the consistent NMR signal intensity of the free and bound Pγ.

Discussion

This paper reports determination of the x-ray crystal structure for the chicken cone PDE6C GAFab regulatory domains. In addition, we employed a number of structural approaches to examine conformational changes in the GAFab structure upon binding of cGMP and/or Pγ, including XL-MS combined with integrative structural modeling, MD simulations (to probe cGMP-induced allostery), and NMR spectroscopy (to identify Pγ residues that interact with GAFab).

The overall x-ray structure depicts prototypical GAFa and GAFb domains with parallel organization of the two subunits, consistent with other GAF-containing PDEs, and shows the greatest structural homology with the homomeric PDE5 GAFab structure {Wang, 2010 #6963}. All of the secondary structure elements in the cone PDE6C GAFa and GAFb domains are closely aligned with those found in the GAFa and GAFb domains of the rod PDE6 catalytic heterodimer {Gulati, 2019 #7980}{Irwin, 2019 #8185}. Similar to rod PDE6, cone PDE6 shows a long GAFa β1/β2 loop extending toward the GAFb domain, a structural feature not found in PDE2 {Martinez, 2002 #7575}. The failure to resolve the GAFb β1/β2 loop region likely reflects the disordered, dynamic nature of this region, and supports the hypothesis that this element may serve as an intermediary in the allosteric communication network originating in the GAFa domain and ending in the catalytic domain. MD simulation results further support conformational changes within this loop region and altered dynamics of this loop on cGMP binding.

XL-MS coupled with integrative structural modeling of cone PDE6C GAFab provided the ability to compare the dynamic solution structure of GAFab to its static crystal structure. Overall, the cross-linked refined apo GAFab structure agrees quite well with the crystal structure but MD simulations provided additional information about flexible regions that may assume different conformations in solution compared to the crystalline state leading to asymmetry in subunits of PDE6 homodimer. Specifically, cross-links identified within the GAFb domain permitted us to develop a structural model for the β1/β2 loop that was not resolved in the x-ray structure. Interestingly, the conformation of the β1/β2 loop in the apo GAFab structural model differs from published crystal structures of other GAF-containing PDEs as well as differing from the cryo-EM structure of bovine rod PDE6 {Gulati, 2019 #7980}. The mobility of this structural element is reflected in the different predicted conformations of the GAFb β1/β2 loop upon binding of cGMP or Pγ (Fig. 4). It appears that in the two states in which Pγ is bound, the β1/β2 loop is oriented in an extended downward conformation (i.e., toward the catalytic domain, were it to be present). We hypothesize that the binding of Pγ to the GAFb domain imposes conformational constraints that may orient it to participate in the proposed allosteric communication network.

Previous studies have shown that binding of cGMP to its noncatalytic binding sites in the GAFa domain is modulated by Pγ binding [reviewed in {Cote, 2006 #5841}]. Both GAFab liganded states that have bound cGMP exhibit conformational changes in the region of the GAFa α4 helix supporting two possible, non-exclusive functional roles: (a) stabilizing cGMP binding by occluding the opening to the binding site to reduce cGMP dissociation; (b) sensing cGMP occupancy and communicating to Pγ or to other structural elements in the allosteric network. Overall, it appears that allosteric communication resulting from the state of occupancy of cyclic nucleotides in noncatalytic sites of GAF domains of GAF-containing PDEs {Martinez, 2002 #4978} may rely on a similar relay of conformationally flexible regions within the GAFab domains. However, in the case of PDE6, it is evident from our comparison of the four GAFab liganded states (Fig. 4) that Pγ plays a dominant role in conveying allosteric changes in the GAF domains to the active sites within the catalytic domains.

The convergence of the NMR and the XL-MS results in locating the major region of Pγ interaction to the GAFb domain (Figs. 7 and 8) is consistent with a role of the GAFb domain as the central hub of allosteric communication, linking cGMP-induced conformational changes the GAFa domain to an as-yet undetermined allosteric communication pathway in the catalytic domain that may be responsible for regulating the catalytic activity of PDE6 at the active site, or perhaps inducing conformational changes in the catalytic domain that alter the affinity with which transducin or RGS9-1 binds. Future efforts will be directed at obtaining additional structural information about the dynamic intra- and inter-molecular communication network of the PDE6 holoenzyme so that the regulation of PDE6 activation lifetime by

the photoreceptor G protein and the RGS9-1 inactivation complex can be integrated with the GAFab allosteric communication network described in this study.

Materials and Methods

Expression and purification of the tandem GAF domains of cone PDE6

The nucleotide sequence corresponding to amino acid residues 42-458 of the chicken cone PDE6 catalytic subunit (UniProtKB P52731) was cloned into the pET47b expression vector containing a C-terminal 6-His fusion tag. The sequence-verified construct was transformed into *E. coli* Rosetta cells and grown at 37 °C in LB media to an OD_{600} of ~0.8. Then, 0.05 mM isopropyl-β-D-1-thiogalactopyranoside was added and the cells incubated at 18 ºC for 18 h. The cell pellet was resuspended in 20 mM Tris, 100 mM NaCl, pH 8.0 and disrupted by sonication. The recombinant protein was purified from the cell extract using a 1 ml HisTrap HP column with the GAFab protein being eluted from the resin with a buffer consisting of 100 mM imidazole, 100 mM NaCl and 20 mM Tris (pH 7.5). The affinity-purified protein was buffer exchanged with 50 mM Tris, 100 mM NaCl, 1 mM β-mercaptoehtanol, 1 mM EDTA, pH 7.5) prior to Superdex 200 gel filtration chromatography. The apparent molecular weight and purity of GAFab was evaluated by sodium dodecyl sulfate-polyacrylamide gel electrophoresis. Protein concentrations were determined by the bicinchoninic acid protein assay {Smith, 1985 #1322} using bovine gamma globulin as standard. Measurements of cGMP binding to GAFab were performed as described previously.

Construction and purification of C-terminal truncated chicken cone Pγ1-58

DNA fragments coding for chicken cone Pγ1-58 was inserted into the *NdeI* and *BamHI* sites of the pET11a vector, followed by transformation into the *E. coli* BL21(DE3) strain. Culture was grown on 2X-TY media at 37ºC until O.D reached 0.6 followed by induction with 0.3mM IPTG. Cells were grown at 30C for 4hr after induction. Following expression, the bacterial extract was purified by HiTrap SP FF column from GE. The Pγ mutants were further purified by C18 reverse-phase high pressure liquid chromatography following standard procedure {Artemyev, 1998 #3585}. The purity of these proteins was determined to be >95% as evaluated by SDS-PAGE. Protein concentrations were evaluated by BCA protein assay using bovine γ-globulin as a standard.

X-ray structure determination

Chicken PDE6C GAF (42-458) protein in concentration of 8 mg/ml was crystallized by the hanging drop method at 4^0C. The drop was prepared by mixing 2 µl PDE6C sample with 2 µl well buffer that contains 0.1 M Na-HEPES pH 7.5, 21-27% PEG3350, 0.2 M ammonium sulfate, and 20% glycerol. The crystals normally show up in 10 d and grow to the maximum size in 4 weeks. The crystals have the space group of

$P6_5$ with cell dimensions of a = b = 148.5, and c = 93.7. The diffraction data of the unliganded PDE6C was collected on the SERCAT beam line of APS and processed by HKL2000 (Otwinowski and Minor, 1997, Table 1). The structure determination was solved by the AutoBuild module of PHENIX (Adams et al., 2010), using the PDE5 GAF as the initial model (Wang et al., 2010). The raw model of PDE6C was rebuilt with program COOT (Emsley et al., 2010) and refined by program REFMAC (Winn et al., 2003, Table 1) to an R-factor of 0.207 for 16489 reflection in the resolution of 50 – 3.2 Å.

Chemical cross-linking, in-gel digestion, and MS analysis

Chemical cross-linking reactions were carried out following the manufacturer's protocols for each cross-linker. PDE6 GAFab was buffer-exchanged into HEPES buffer (20 mM HEPES, 100 mM NaCl, 5 mM $MgCl_2$, pH 8.0) and incubated with Pγ or/and cGMP. After incubating with cross-linker at RT for 1 h, proteins were separated with NuPAGE 4-12% Bis-Tris gels and visualized with Coomassie Brilliant Blue G-250.

Bands representing cross-linked proteins were in-gel digested and analyzed by LC-MS and LC-MS/MS as essentially described previously {Zeng-Elmore, 2014 #7444}. Briefly, the protein bands were excised from the SDS-PAGE gel and washed with 25 mM NH_4HCO_3/50% acetonitrile (ACN) to remove the Coomassie stain. Reduction of disulfide bonds were carried out by treating with 10mM DTT and later on cysteine alkylation was done with 55 mM iodoacetamide prepared in 25 mM NH_4HCO_3. Samples were dries out in speed vaccum. Dried gel pieces were treated with trypsin and asp-N (Promega) to cleave proteins in to peptides. The digested peptides were extracted from the gel pieces using 50%ACN, 20%formic acid and 100%ACN solution in sequential manner and concentrated to ~7 µl using the Speedvac. One microliter aliquots of the concentrated peptides were injected into the Dionex Ultimate 3000 RSL Cnano UHPLC system (Dionex Corporation Sunnyvale, CA) and separated by a 75 µm × 25 cm PepMAp RSLC column (100 Å, 2 µm) at a flow rate of ~450nl/min (mobile phase A:0.1% formic acid in H_2O, mobile phase B:0.1% formic acid in 80% acetonitrile). The eluant was connected directly to a nano electrospray ionization source of an LTQ Orbitrap XL mass spectrometer (Thermo Scientific,Waltham,MA). LC-MS data were acquired in an information-dependent acquisition mode. Full MS spectra were acquired in the Orbitrap (m/z 315-2000) with a resolution of 30000 at m/z 400. The five most intense ions were selected for collision-induced dissociation (CID) fragmentation in the linear ion trap for MS/MS data acquisition.

Cross-linked peptide identification

Cross-linked peptides were identified using an integrated module in Protein Prospector, based on a bioinformatic strategy described previously {Chu, 2010 #7046;Trnka, 2014 #8096}. The score of a cross-linked peptide was based on the number and types of fragments ions identified, as wells as the sequence and the charge state of the cross-linked peptides. Only results where the score difference is greater than 0 (i.e the cross-linked peptide match was better than a single peptide match alone) are considered. The expectation values are calculated based on matches to single peptides and thus should be treated as another score, rather than a statistical measure of reliability.

Structural modeling

The GAFab x-ray crystal structure was used as template and cross-linking data was applied as distance restraints in Modeller v9.11 to obtain the cross-link refined solution structure of GAFab under all four condition as discussed above. Symmetry was enforced for the two subunits. The comparative model with lowest DOPE score (out of 10) was selected.

To perform docking of Pγ to GAFab, the Integrated Modeling Platform [IMP; {Sali, 1993 #7154}] was used with GAFab considered as a single rigid body, and Pγ residues 23-50 treated as a rigid body. The homologous Pγ residues from rod PDE6 holoenzyme {Irwin, 2019 #8185} were used as a template for initial docking, and IMP was run with a high temperature of 2.0, a low temperature of 0.5, and using a new system configuration at each step. The top 100 scoring models were generated and saved, and IMP was then used to perform clustering on the top 100 models in order to aid in model selection. The best fitting model was run in Modeller using the same cross-linking restraints in order to further refine the model, evaluate stereochemical quality, and fill in the missing atoms. Secondary structure identification was initially determined by Pymol version 2.3 (Schrodinger).

To evaluate potential differences between the two subunits of GAFab and to assess conformational changes occurring upon ligand binding, analysis of the root mean square deviations (RMSD) of our structural model with other available structures was carried out using Visual Molecular Dynamics (VMD) software version 1.9.3 {Humphrey, 1996 #8076}.

System setup and MD simulation details

The software Visual Molecular Dynamics (VMD) {Humphrey, 1996 #8076} was used to prepare all systems and analyze simulation trajectories. All simulations were performed using the NAMD software {Phillips, 2005 #7709} with three different structures of GAFab: The x-ray structure and the structural models (consisting of residues 42-458) of the unliganded (apo) and cGMP-bound GAFab states. We note that the x-ray structure PDE6 does not contain a portion of the GAFb β1/β2 flexible loop (residues 286-310), whereas the two cross-link refined structural models include this loop. In the cGMP-bound structural

model, a cGMP molecule was docked in each GAFa binding site based on the atomic coordinates of cGMP reported for the published chicken cone GAF structure (PDB ID: 3DBA).

The three structures were solvated with TIP3P water molecules and the systems were neutralized with NaCl and $MgCl_2$. After 500 steps of conjugate-gradient minimization, we equilibrated the volume of the simulation domain for each system by conducting a short 1 ns MD simulation in the NPT ensemble, after which we conducted three independent long time-scale MD simulations of each system (Table S1). In all simulations, we used a time-step of 2 fs and the CHARMM force-field for all molecules {MacKerell, 1998 #7714;Mackerell, 2004 #7715;Huang, 2017 #8094}. The temperature was maintained (at 310 K) using a Langevin thermostat and the pressure (at 1 atm) using a Nosé-Hoover barostat.

MD conformational metrics

Root Mean Squared Deviation/Fluctuation (RMSD/RMSF): To understand the domain-level flexibility of PDE6 in various states (crystal structure, apo, and cGMP-bound states), we computed the RMSD as a metric based on the Cα atoms, where RMSD was measured relative to the initial structure in each simulation. A higher RMSD relative to the initial structure would indicate increased flexibility and vice-versa. The probability distributions of RMSDs of various domains of PDE6 are shown in Figs. S6-S8. To quantify the conformational flexibility of each residue, we further computed RMSF per residue for each subunit of PDE6. The RMSF calculations were based on all atoms in each residue. The RMSF data are shown in Figs. S6-S8.

Buried surface area (BSA): To characterize interfacial area between a pair of domains within PDE6, we calculated BSA between domains using the following equation: $\mathrm{BSA} = \mathrm{SASA_a} + \mathrm{SASA_{a'}} - \mathrm{SASA_{aa'}}$

where $\mathrm{SASA_a}$, $\mathrm{SASA_{a'}}$, and $\mathrm{SASA_{aa'}}$ are the solvent-accessible surface areas (SASA) of each domain individually or both domains taken together. We used a probe radius of 1.4 Å for SASA calculations.

Interdomain distances: To quantify the relative movement of individual domainsof PDE6, we measured distances between the center-of-mass (COM) of the following six pairs of domains in the homodimer: GAFa-GAFa'; GAFb-GAFb'; GAFa-GAFb; GAFa'-GAFb'; GAFa-GAFb'; and GAFa'-GAFb.

Dynamic Cross Correlation (DCC) Analysis: We also carried out residue-residue (Cα-Cα) DCC analysis for different states of PDE6. Specifically, for a pair of atoms *i* and *j*, the correlation coefficient C*ij* was computed using time-averaged displacements (Δr_i and Δr_j) from the mean positions.

NMR spectroscopy

Uniformly ^{13}C, ^{15}N enriched Pγ was produced by expressing the protein in M9 minimal medium supplemented with $^{15}NH_4Cl$ and $^{13}C_6$-glucose (for uniform labeling with nitrogen-15 and carbon-13), respectively. After purification, Pγ was resuspended in a buffer containing 20 mM Tris, 50 mM NaCl, 1 mM $MgCl_2$, pH 7.5. D_2O, NaN_3, and DSS were added for a final concentration of 5% v/v, 1 mM, and 200 μM, respectively. NMR spectra were collected at 25 °C on a Bruker Avance III HD 700 MHz NMR spectrometer equipped with a quadruple resonance inverse QCI-F CryoProbe at the City University of New York Advanced Science Research Center (CUNY ASRC) Biomolecular NMR Facility and on a Bruker Avance NEO 700 MHz NMR spectrometer equipped with a 5-mm triple resonance inverse TCI CryoProbe at the University of New Hampshire Instrumentation Center NMR facility. For backbone and sidechain assignments, 2D ^{1}H-^{15}N HSQC, and 3D HNCA, HNCACB, and HNCO spectra were collected of 50 μM uniformly ^{13}C,^{15}N enriched Pγ. To investigate the binding properties of Pγ and GAFab, uniformly ^{13}C,^{15}N enriched Pγ (20 μM) and natural abundance GAFab (72 μM) were mixed, and 2D ^{1}H-^{15}N HSQC spectra of Pγ were acquired (with and without GAFab). All NMR data were processed using NMRPipe {Delaglio, 1995 #8193}. Analysis and assignments of the 2D and 3D data sets were carried out using NMRFAM-Sparky {Lee, 2015 #8194}. The assignment process was facilitated by using the PINE server for initial automated assignments {Bahrami, 2009 #8192}{Lee, 2009 #8195} before completing the assignments manually.

Acknowledgements. We thank Suzanne L. Matte for assistance with the preparation of proteins used in this study, Dr. Karyn B. Cahill for the initial work on optimizing expression of the GAFab protein, and Dr. James Aramini (City University of New York Advanced Science Research Center (CUNY ASRC) Biomolecular NMR Facility) for his assistance with the NMR data collection. This work was supported by the National Eye Institute grant R01 EY05798 (R.H.C.), the National Institute of General Medical Sciences grants P20 GM113131 (R.H.C.) and GM059791 (H.K.), P20GM103449 (Vermont Genetics Network Proteomics Core Facility), National Science Foundation grant CLF 1307367 (F.C.), National Institute of Child Health and Human Development grant R01 HD093783 (F.C.), National Science Foundation Major Research Instrumentation Award DBI-1828319 (K.V.). The computations were performed in part using the NSF-supported (ACI-1548562) Extreme Science and Engineering Discovery Environment (XSEDE) Comet resource at San Diego Supercomputer Center under grant TGMCB160183 (H.V.) and the National Science Foundation EPSCoR grant OIA-1757371 (H.V). Institutional support was provided through UNH CoRE grant (H.V., F.C, R.H.C., and K.V.) and through the UNH Research Computing Center central shared HPC Premise cluster (H.V.).

Table 1. Statistics on diffraction data and structure refinement of Unliganded PDE6C

Data collection	
Space group	$P6_5$
Unit cell (a = b. c, Å)	148.5, 148.5, 93.7
Resolution (Å)	3.2
Wave length (Å)	1.0
Unique reflections	16,737
redundancy	4.8 fold
Completeness (%)	86.0 (87.7)*
Average I/σ	6.2 (1.9)*
Rmerge	0.142 (0.712)*
Refinement	
R-factor	0.207
R-free	0.308 (5.0%)‡
Resolution (Å)	50-3.2
Bond (Å)	0.011
Angle	1.65°
Protein	72.5 (6251)§
Ramachandran Plot	
Most favored	94.0
Allowed	5.8
Generally allowed	0.2

*The numbers in parentheses are for the highest resolution shell.
‡The percentage of reflections omitted for calculation of R-free.
§The number of atoms in the crystallographic asymmetric unit.

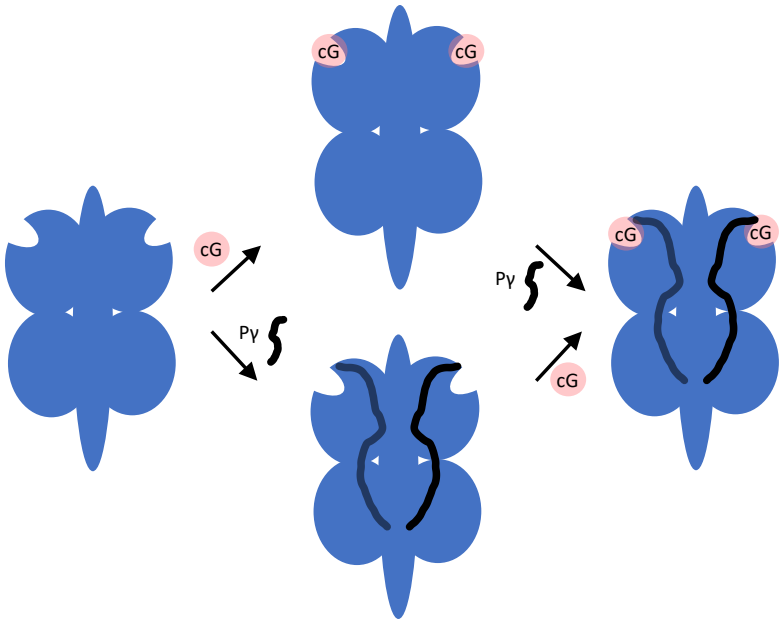

Fig. 1. Multiple equilibria of ligand binding to PDE6 regulatory GAFab domains. The two tandem GAF domains (GAFa and GAFb) are denoted with blue circles, and the long helical regions and N- and C-termini collectively denoted as an elongated ellipsoid. cGMP binding to the GAFa domain is represented by red circles. The inhibitory Pγ subunit is depicted as a black line.

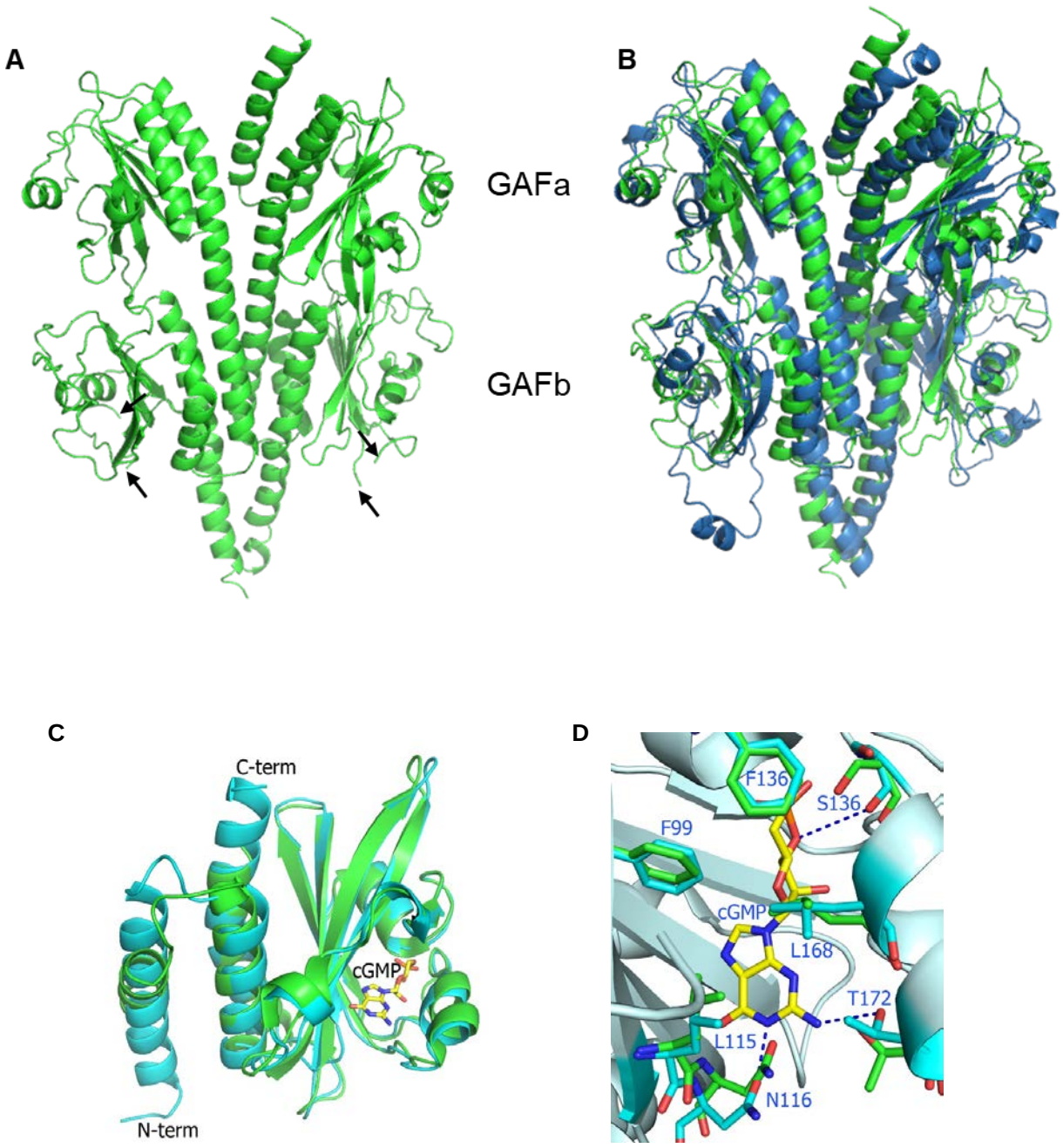

Fig 2. Structure of cone PDE6 regulatory domains. A. X-ray structure of chicken cone PDE6 GAFab at 3.3 Å resolution. Arrows indicate location of unresolved loop structure in the GAFb domain. **B.** Comparison of x-ray structure of cone PDE6 GAFab (green) with rod PDE6 catalytic dimer [dark blue; {Irwin, 2019 #8185}]. (C). Structural alignment of cone GAFa (green) x-ray structure with bovine rod PDE6 β-subunit GAFa domain (cyan; Irwin et al., 2019). (D) Changes of the cGMP binding residues. Cyan sticks represent the residues in the crystal structure of PDE6C-cGMP, while the corresponding residues of the unliganded PDE6C are shown as green sticks. The dotted lines represent the hydrogen bonds.

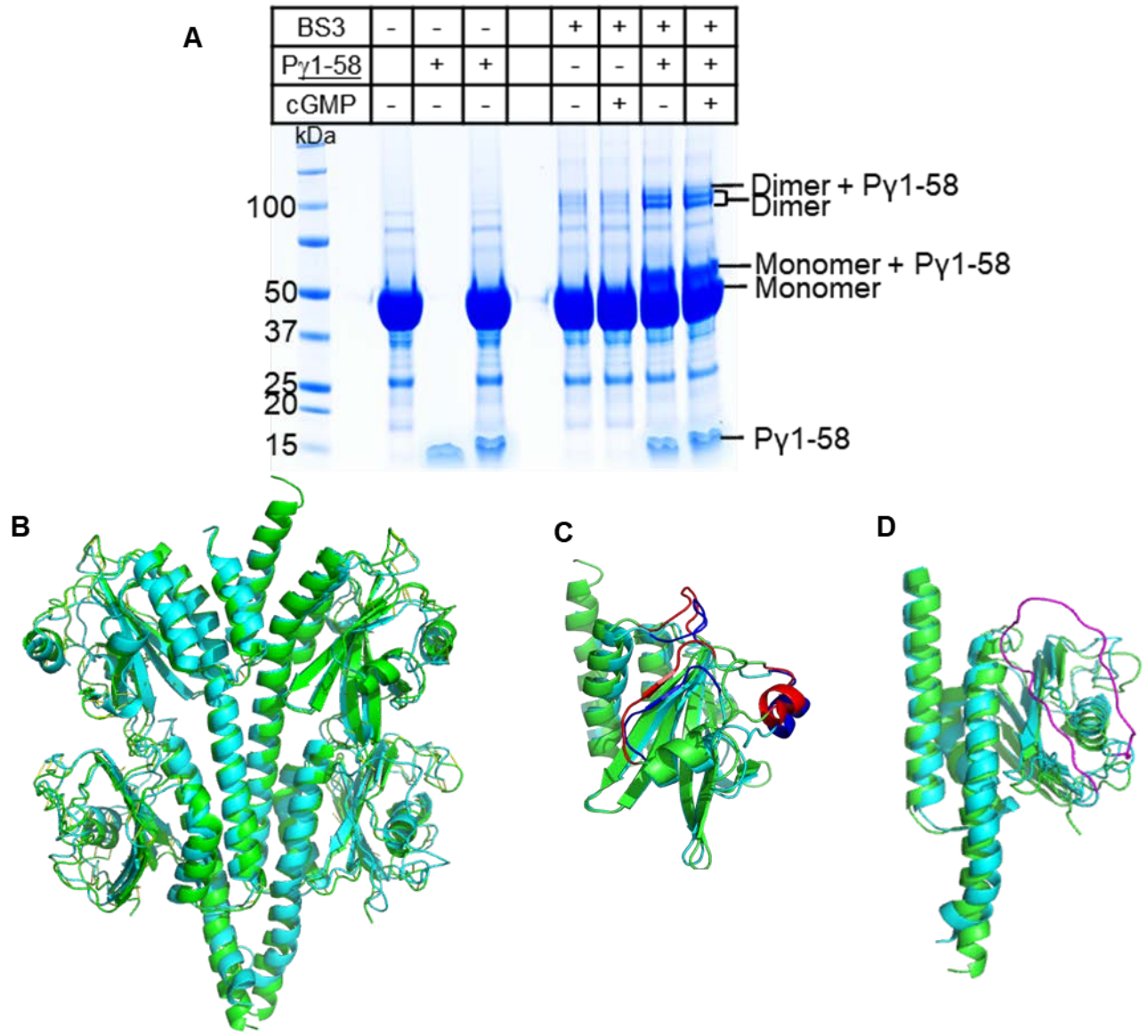

Fig 3. Solution structure of the apo state of cone PDE6 GAFab determined by cross-linking mass spectrometry. A. SDS-PAGE of a cross-linking experiment in which 12 µM GAFab was incubated in the presence or absence of cGMP(10 fold molar excess) and/or 120 µM Pγ1-58 prior to addition of a 50-fold molar excess of the chemical cross-linker BS3. **B.** Structural alignment of cross-linked refined apo-GAFab (cyan) with x-ray structure (green). **C.** Superimposition of the GAFa domain of x-ray structure (green) and the apo structural model (cyan), with major differences indicated for the x-ray (red) and apo (blue). **D.** Superimposition of the GAFb domain of the x-ray structure (green) and the apo structure (cyan), with the β1/β2 loop (residues 285 to 310) of the apo structure highlighted in magenta that is missing in the x-ray structure.

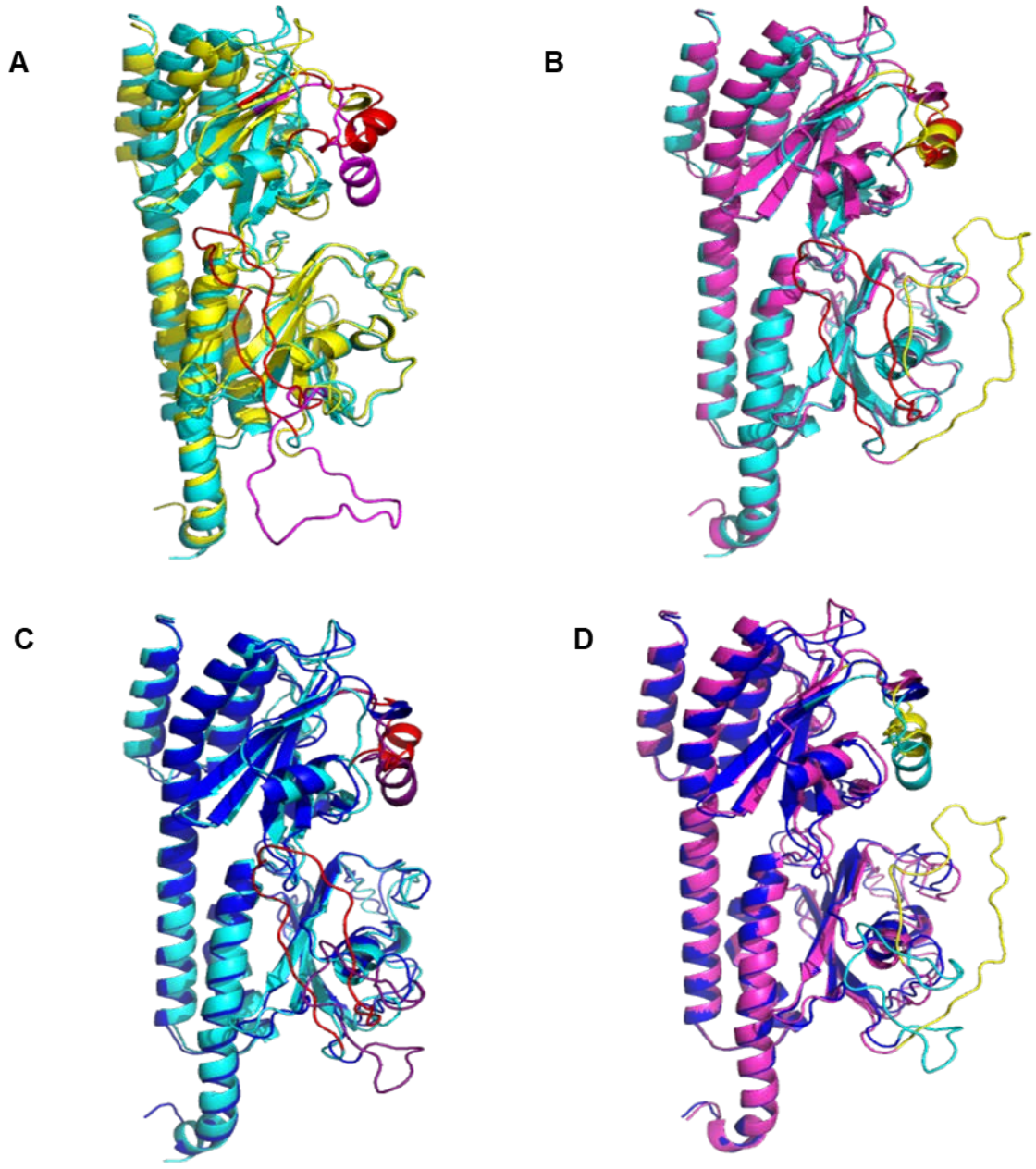

Fig 4. Structural models for PDE6 GAFab in various liganded states. A. Superimposition of GAFab in its apo (cyan) and Pγ-bound (yellow) states; significant structural differences are highlighted with red (apo) or magenta (Pγ bound). **B.** Comparison of apo GAFab (cyan) with cGMP-bound GAFab (magenta); differences are highlighted with red (apo) or yellow (cGMP bound). **C.** Superimposition of GAFab in its apo state (cyan) or with both Pγ and cGMP bound (blue); significant differences highlighted with red (apo) or purple (cGMP and Pγ bound). **D.** Comparison of the cGMP bound state of GAFab with (blue) or without (magenta) bound Pγ1-58; structural differences are highlighted in yellow (cGMP bound) or cyan (cGMP and Pγ bound).

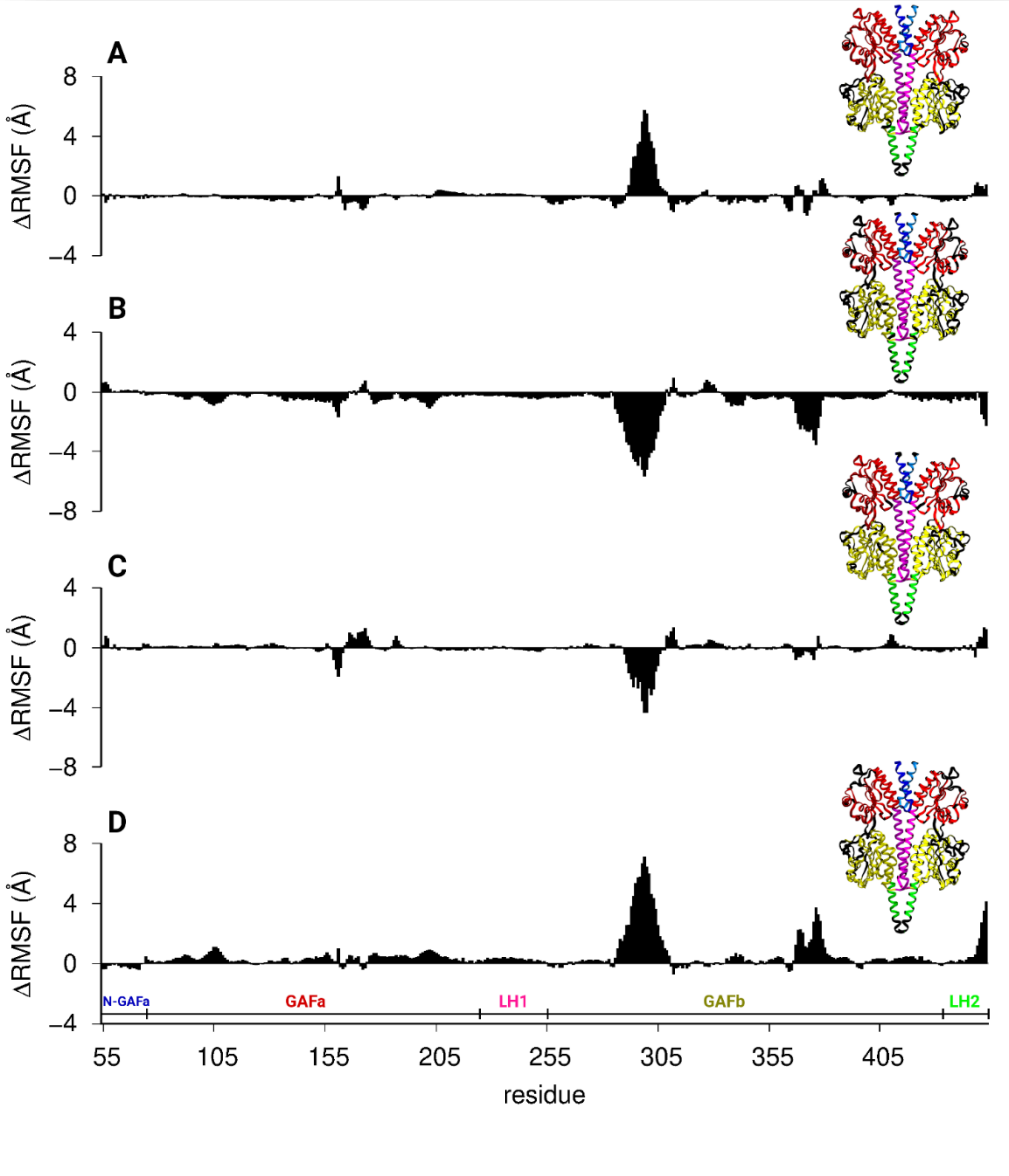

Fig. 5. Molecular dynamics (MD) simulations of the apo and cGMP-liganded states of GAFab. Differences in the root mean squared fluctuations (ΔRMSF) per residue were analyzed separately for each sub-domain of GAFab [N-terminal region of GAFa (N-GAFa, residues 55-74), GAFa (residues 75-224), long helix-1 (LH1, residues 225-255), GAFb (residues 256-443), and long helix-2 (LH2, residues 434-453) to identify differences in protein dynamics of the apo and cGMP-bound states for each subunit. Any regions that differed more than 0.5 Å are highlighted in black on the accompanying structure. **A and B.** Evaluation of asymmetry in protein dynamics of the two GAFab subunits in the apo (panel A) and cGMP-bound (panel B) state. **C and D.** Changes in protein dynamics upon cGMP binding to each subunit of GAFab were evaluated by plotting the ΔRMSF per residue for the apo and cGMP-liganded states for subunit A (panel C) and subunit B (panel D).

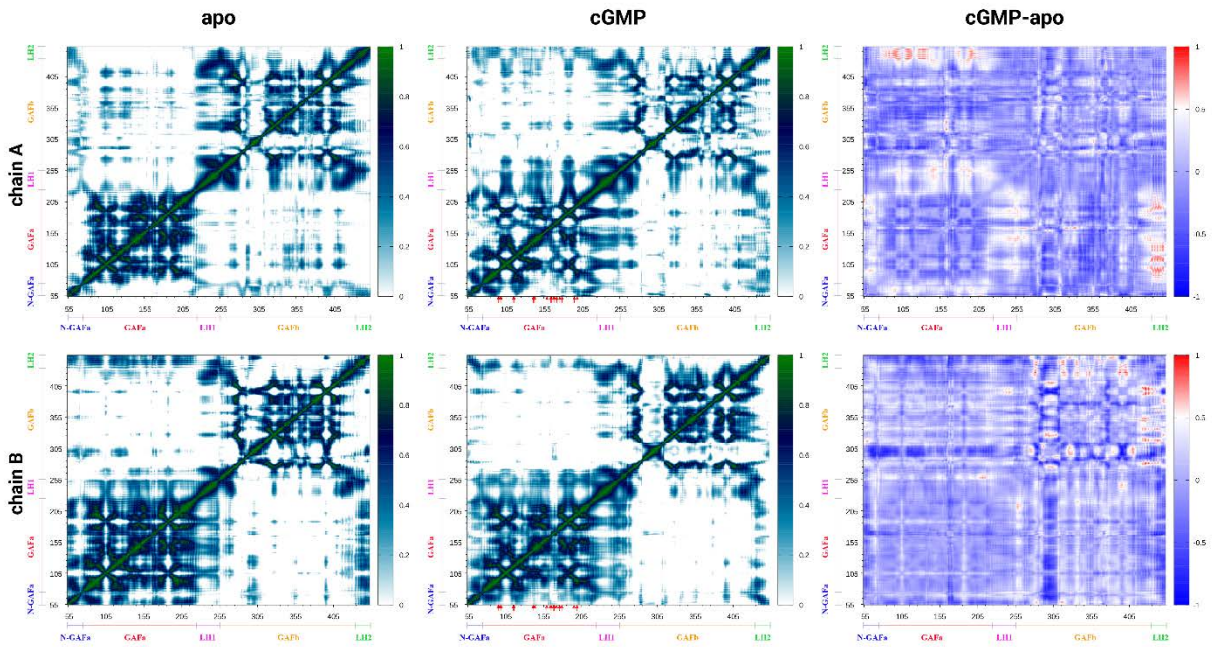

Fig. 6. Dynamic cross-correlation (DCC) analysis of the apo and cGMP-liganded states of GAFab. (*top*) DCC maps corresponding to chain A and (*bottom*) DCC maps corresponding to chain B. The maps in the right-most panels are the difference between the cGMP-liganded states and the apo-states. Color bars indicated the range of correlations between 0 (no correlation) and 1 (high correlations).

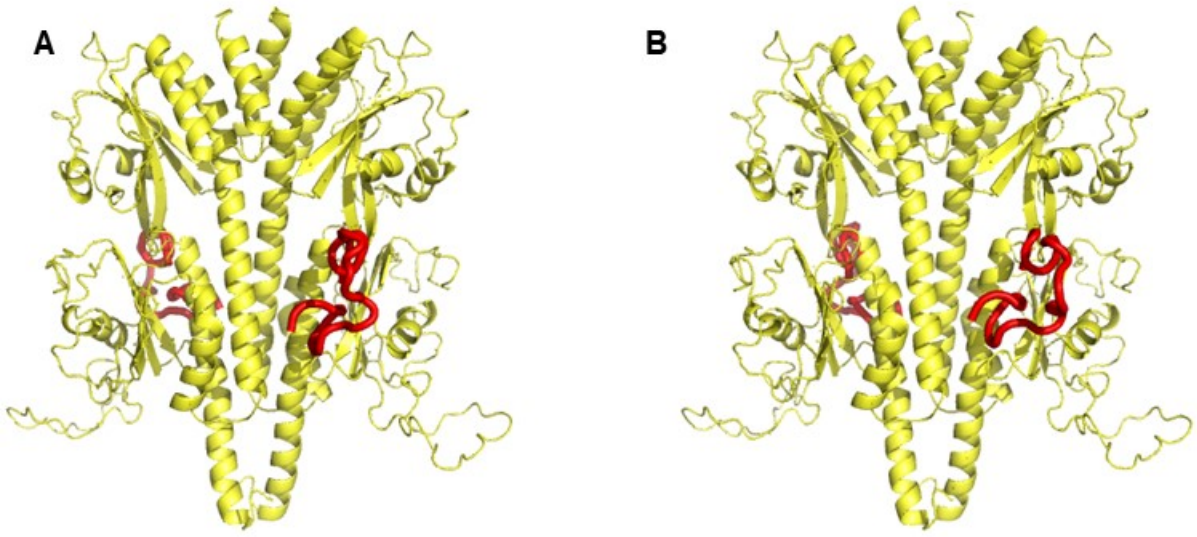

Fig. 7. Integrative structural model of a fragment of cone Pγ complexed with PDE6 GAFab. The Integrative Modelling Platform was used to dock cone Pγ (residues 23 to 50; shown as thick red lines) to GAFab, using the structural model for the corresponding region of bovine rod Pγ as template {Irwin, 2019 #8185}, and applying spatial restraints obtained from data for cross-linked peptides obtained in this region of the Pγ sequence. **A.** Pγ23-50 interacts with the GAFb domain of chain A**. B.** 180º rotation of Figure A showing the second Pγ23-50 fragment docked to Chain B of GAFab.

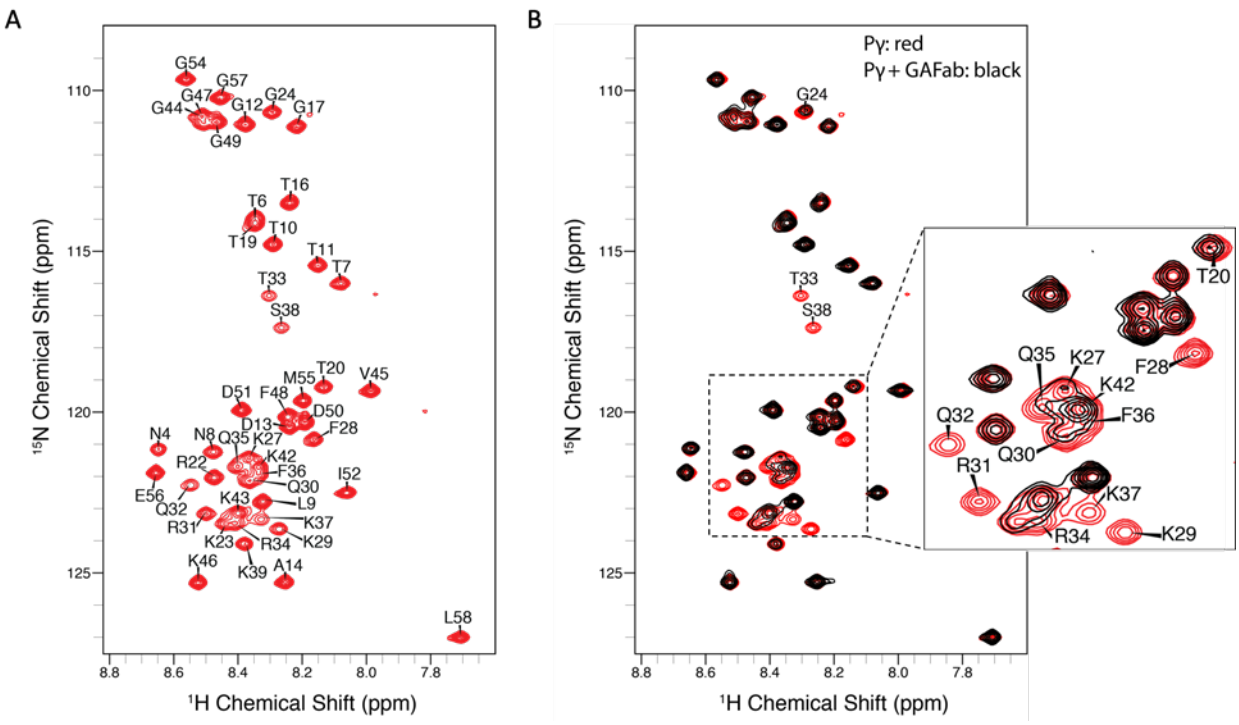

Fig. 8. Pγ1-58 NMR resonance assignments and binding studies. (A) 2D ^{1}H-^{15}N HSQC NMR spectrum of Pγ in its unbound state. Narrow dispersion of ^{1}H chemical shifts between 9.0 and 7.5 ppm is indicative of an intrinsically disordered protein. (B) The overlay of the 2D ^{1}H-^{15}N HSQC NMR specta of the unbound Pγ (red spectrum) and Pγ bound to GAFab (black spectrum) illustrates that the addition of GAFab induced significant changes in the Pγ spectrum. The most significant line broadening was observed in the F28-S38 region of Pγ, indicative of the binding interface.

Supplementary Information for

Allosteric regulation of cone photoreceptor phosphodiesterase (PDE6) by cGMP and PDE6 inhibitory γ-subunit binding to the GAF domains

Richa Gupta, Yong Liu, Huanchen Wang, Christopher T. Nordyke, Ryan Z. Puterbaugh, Krisztina Varga, Feixia Chu, Hengming Ke, Harish Vashisth, and Rick H. Cote

Corresponding author: Rick H. Cote
Email: rick.cote@unh.edu

This PDF file includes:

Table S1. Cross-links identified for the apo state of PDE6C GAFab.

m/z	z	ppm	aa1	aa2	crosslinker
901.8438	3	3.3	395	396	Sulfo-SDA
1045.559	4	3.2	130	132	Sulfo-SDA
644.8098	4	14	263	450	Sulfo-SDA
516.0494	5	14	263	451	Sulfo-SDA
516.0497	5	14	263	452	Sulfo-SDA
514.6675	5	-0.061	160	163	Sulfo-SDA
1024.541	4	-15	130	214	Sulfo-SDA
1018.069	4	3.7	395	396	BS3
710.1106	4	6.1	288	305	BS3
947.9791	4	1.7	283	288	EDC
868.4985	3	9.8	395	398	EDC
516.0494	5	1.3	446	449	EDC
979.0488	4	3.8	395	397	EDC
650.0952	4	3	157	160	EDC
738.3666	4	2.6	289	305	EDC
815.715	7	5.9	150	179	EDC
562.5233	4	-0.091	160	368	Sulfo-SDA
567.1266	5	0.4	396	398	Sulfo-SDA
516.7652	4	-0.26	160	210	Sulfo-SDA
530.797	4	1.1	328	329	Sulfo-SDA
601.3285	4	-0.72	263	446	Sulfo-SDA
591.1158	5	-0.51	329	409	Sulfo-SDA
439.732	4	-0.2	263	439	Sulfo-SDA
708.6566	4	0.6	395	397	Sulfo-SDA
570.2784	4	1.4	234	412	Sulfo-SDA
524.5365	4	1	263	252	Sulfo-SDA
575.045	4	0.83	263	416	Sulfo-SDA
630.6795	3	0.33	263	264	Sulfo-SDA
545.5443	4	0.33	258	319	Sulfo-SDA
486.2567	4	-0.71	78	80	Sulfo-SDA
607.0844	4	1.3	133	150	Sulfo-SDA
539.7915	4	-0.81	95	160	Sulfo-SDA
609.0884	4	2.9	109	150	Sulfo-SDA
486.2571	4	0.12	77	82	Sulfo-SDA
524.5365	4	1	252	263	Sulfo-SDA
568.657	3	-0.74	395	439	Sulfo-SDA
486.2567	4	-0.71	78	80	Sulfo-SDA
522.4997	4	-0.9	288	293	Sulfo-SDA
570.2784	4	1.4	234	412	Sulfo-SDA
545.5443	4	0.33	258	319	Sulfo-SDA
630.6795	3	0.33	263	264	Sulfo-SDA

Crosslinking conditions were followed as described in Fig. 3. Cross-linked peptides were identified following chemical cross-linking of apo GAFab and analyzed as described in *Methods*. Exp. m/z is the experimentally measured mass-to-charge ratio, z is the charge state of the peptide, and Δ is the accuracy measured in parts per million. The crosslinked peptides are defined by amino acid residue number (aa1, aa2) identified using the indicated crosslinker.

Table S2. Cross-links identified for the cGMP-liganded state of PDE6C GAFab.

m/z	z	ppm	aa1	aa2	crosslinker
901.8419	3	1.2	395	396	Sulfo-SDA
907.1179	3	2.5	286	288	Sulfo-SDA
1075.893	3	5.1	132	133	Sulfo-SDA
644.8436	2	1.2	305	306	Sulfo-SDA
644.8104	4	15	263	450	Sulfo-SDA
516.0493	5	14	263	452	Sulfo-SDA
516.0497	5	14	263	451	Sulfo-SDA
605.6481	3	0.79	308	311	Sulfo-SDA
688.8895	2	2.3	263	264	Sulfo-SDA
1045.561	4	5.4	132	138	Sulfo-SDA
680.8263	4	-14	169	308	Sulfo-SDA
488.7177	4	-4.1	151	170	Sulfo-SDA
710.1086	4	3.3	288	305	BS3
728.1359	4	4.6	159	180	BS3
947.9793	4	1.9	283	288	EDC
516.0505	5	3.4	446	449	EDC
911.1931	3	5.2	395	398	EDC
650.0953	4	3.2	157	160	EDC
738.368	4	4.5	289	308	EDC
430.8685	3	-1.1	286	287	Sulfo-SDA
486.2574	4	0.73	78	80	Sulfo-SDA
473.2619	4	1.5	263	264	Sulfo-SDA
473.2616	4	0.82	259	263	Sulfo-SDA
492.5123	4	2.1	258	319	Sulfo-SDA

Crosslinking conditions were followed as described in Fig. 3 Cross-linked peptides were identified following chemical cross-linking of GAFab pre-incubated with cGMP and analyzed as described in *Methods*. Abbreviations are defined in the legend to Table S1.

Table S3. Cross-links identified for the Pγ-liganded state of PDE6C GAFab.

m/z	z	ppm	pep1	aa1	pep2	aa2	crosslinker
901.8422	3	1.5	GAFab	395	GAFab	396	Sulfo-SDA
1045.558	4	1.7	GAFab	130	GAFab	132	Sulfo-SDA
870.1294	3	-1.3	GAFab	263	GAFab	264	Sulfo-SDA
516.0483	5	12	GAFab	263	GAFab	452	Sulfo-SDA
708.6545	4	-2.4	GAFab	396	GAFab	408	Sulfo-SDA
605.6467	3	-1.5	GAFab	308	GAFab	311	Sulfo-SDA
868.4924	3	2.7	GAFab	395	GAFab	397	EDC
868.4937	3	4.2	GAFab	395	GAFab	398	EDC
866.4572	3	2.3	GAFab	157	GAFab	160	EDC
758.5859	5	3.3	GAFab	286	GAFab	289	EDC
947.98	4	2.7	GAFab	283	GAFab	288	EDC
516.0495	5	1.5	GAFab	446	GAFab	449	EDC
722.6653	4	3.5	GAFab	395	GAFab	396	BS3
1024.528	3	0.0031	GAFab	132	GAFab	171	BS3
517.0277	4	-0.45	GAFab	263	GAFab	441	BS3
687.1057	4	-0.2	GAFab	78	GAFab	122	BS3
464.6031	3	1	GAFab	151	GAFab	169	BS3
504.0407	4	-0.15	GAFab	396	GAFab	441	BS3
611.3097	3	-4.3	GAFab	132	GAFab	160	BS3
599.6564	3	4.3	GAFab	151	GAFab	214	BS3
605.3181	3	-0.39	GAFab	319	GAFab	441	BS3
646.8674	2	2	GAFab	151	GAFab	170	BS3
427.9638	4	-1.3	GAFab	441	GAFab	444	BS3
751.768	3	1.8	GAFab	385	GAFab	386	Sulfo-SDA
1047.882	3	2.3	GAFab	188	GAFab	189	Sulfo-SDA
786.1621	4	0.69	GAFab	188	GAFab	190	Sulfo-SDA
901.8417	3	0.95	GAFab	396	GAFab	397	Sulfo-SDA
708.6566	4	0.58	GAFab	396	GAFab	400	Sulfo-SDA
727.0612	3	0.53	GAFab	199	GAFab	200	Sulfo-SDA
902.1306	3	1.8	GAFab	156	GAFab	171	Sulfo-SDA
730.3585	2	0.0019	GAFab	78	GAFab	79	Sulfo-SDA
674.8718	2	0.34	GAFab	122	GAFab	123	Sulfo-SDA
715.8451	2	-0.63	GAFab	374	GAFab	375	Sulfo-SDA
632.3214	2	-0.51	GAFab	444	GAFab	445	Sulfo-SDA
482.2609	3	-0.052	GAFab	328	GAFab	329	Sulfo-SDA
707.3934	3	0.88	GAFab	328	GAFab	330	Sulfo-SDA
707.3923	3	-0.68	GAFab	328	GAFab	333	Sulfo-SDA
850.9415	2	0.93	GAFab	130	GAFab	132	Sulfo-SDA
644.8423	2	-0.79	GAFab	305	GAFab	306	Sulfo-SDA
988.9966	2	0.39	GAFab	132	GAFab	134	Sulfo-SDA
988.9964	2	0.19	GAFab	132	GAFab	135	Sulfo-SDA
760.0797	3	1.3	GAFab	122	GAFab	135	Sulfo-SDA
819.9417	2	1.4	GAFab	256	GAFab	319	Sulfo-SDA
568.6575	3	0.078	GAFab	395	GAFab	439	Sulfo-SDA
681.7285	3	-1.3	GAFab	255	GAFab	395	Sulfo-SDA
632.3215	2	-0.35	GAFab	441	GAFab	446	Sulfo-SDA
547.838	2	0.61	GAFab	82	GAFab	83	Sulfo-SDA
1006.506	2	0.51	GAFab	249	GAFab	250	Sulfo-SDA
743.8929	2	-0.18	GAFab	305	GAFab	308	Sulfo-SDA
707.3939	3	1.6	GAFab	327	GAFab	332	Sulfo-SDA
738.4125	3	0.59	GAFab	211	GAFab	215	Sulfo-SDA
699.0277	3	-1.6	GAFab	150	GAFab	170	Sulfo-SDA
752.1006	3	-8.2	GAFab	132	GAFab	386	Sulfo-SDA
593.572	4	0.23	GAFab	151	GAFab	209	Sulfo-SDA
430.2307	3	-0.62	GAFab	304	GAFab	308	Sulfo-SDA

Crosslinking conditions were followed as described in Fig. 3. Cross-linked peptides were identified following chemical cross-linking of GAFab pre-incubated with Pγ and analyzed as described in *Methods*. Abbreviations are defined in the legend to Table S1.

Table S4. Cross-links identified for the Pγ- and cGMP-liganded state of PDE6C GAFab.

m/z	z	ppm	pep1	aa1	pep2	aa2	crosslinker
579.2989	4	-0.43	GAFab	396	GAFab	441	BS3
1024.528	3	0.3	GAFab	132	GAFab	171	BS3
595.8455	4	0.13	GAFab	82	GAFab	122	BS3
413.8239	5	0.24	GAFab	263	GAFab	441	BS3
813.7858	3	-0.26	GAFab	263	GAFab	319	BS3
528.5142	5	-0.91	GAFab	263	GAFab	396	BS3
695.0345	3	-0.14	GAFab	319	GAFab	444	BS3
605.3187	3	0.61	GAFab	319	GAFab	441	BS3
464.6026	3	-0.048	GAFab	151	GAFab	159	BS3
687.1059	4	0.09	GAFab	78	GAFab	122	BS3
599.6541	3	0.46	GAFab	151	GAFab	214	BS3
751.7666	3	-0.022	GAFab	385	GAFab	386	Sulfo-SDA
901.8412	3	0.4	GAFab	385	GAFab	387	Sulfo-SDA
1047.881	3	0.9	GAFab	188	GAFab	189	Sulfo-SDA
821.0855	3	2.7	GAFab	168	GAFab	171	Sulfo-SDA
766.4034	3	-1.5	GAFab	103	GAFab	171	Sulfo-SDA
1018.539	3	0.68	GAFab	95	GAFab	171	Sulfo-SDA
708.6578	4	2.3	GAFab	396	GAFab	397	Sulfo-SDA
901.8425	3	1.8	GAFab	395	GAFab	396	Sulfo-SDA
676.6326	4	0.22	GAFab	393	GAFab	396	Sulfo-SDA
574.6073	3	0.94	GAFab	367	GAFab	412	Sulfo-SDA
730.3586	2	0.14	GAFab	78	GAFab	79	Sulfo-SDA
722.8879	2	0.21	GAFab	328	GAFab	329	Sulfo-SDA
361.9468	4	-2	GAFab	328	GAFab	330	Sulfo-SDA
973.8683	3	1.3	GAFab	132	GAFab	216	Sulfo-SDA
630.6799	3	1	GAFab	263	GAFab	264	Sulfo-SDA
1084.557	2	0.42	GAFab	249	GAFab	250	Sulfo-SDA
644.8433	2	0.76	GAFab	305	GAFab	306	Sulfo-SDA
787.054	3	-0.77	GAFab	374	GAFab	378	Sulfo-SDA
787.0552	3	0.76	GAFab	374	GAFab	379	Sulfo-SDA
1060.587	2	1.2	GAFab	328	GAFab	333	Sulfo-SDA
988.9967	2	0.49	GAFab	132	GAFab	134	Sulfo-SDA
681.7287	3	-1	GAFab	255	GAFab	395	Sulfo-SDA
1006.506	2	0.51	GAFab	249	GAFab	251	Sulfo-SDA
674.8718	2	0.34	GAFab	122	GAFab	123	Sulfo-SDA
977.5193	3	1.2	GAFab	122	GAFab	126	Sulfo-SDA
632.322	2	0.44	GAFab	441	GAFab	445	Sulfo-SDA
988.9957	2	-0.52	GAFab	132	GAFab	133	Sulfo-SDA
659.6673	3	1.1	GAFab	132	GAFab	135	Sulfo-SDA
988.9973	2	1.1	GAFab	130	GAFab	132	Sulfo-SDA
715.8455	2	-0.07	GAFab	374	GAFab	375	Sulfo-SDA
743.8934	2	0.5	GAFab	305	GAFab	308	Sulfo-SDA
653.7973	2	0.14	GAFab	286	GAFab	288	Sulfo-SDA
568.6575	3	0.078	GAFab	395	GAFab	439	Sulfo-SDA
681.7287	3	-1	GAFab	255	GAFab	395	Sulfo-SDA
648.6512	3	0.26	GAFab	257	GAFab	374	Sulfo-SDA
819.9401	2	-0.5	GAFab	258	GAFab	319	Sulfo-SDA
577.9899	3	1.4	GAFab	395	GAFab	415	Sulfo-SDA
707.3931	3	0.45	GAFab	327	GAFab	332	Sulfo-SDA
547.8376	2	-0.12	GAFab	82	GAFab	83	Sulfo-SDA
363.8491	3	0.37	GAFab	161	GAFab	170	Sulfo-SDA
514.6675	5	-0.061	GAFab	160	GAFab	163	Sulfo-SDA
868.4938	3	4.3	GAFab	395	GAFab	397	EDC
650.0968	4	5.5	GAFab	157	GAFab	160	EDC
793.4263	3	5.9	GAFab	311	GAFab	319	EDC
947.981	4	3.7	GAFab	283	GAFab	288	EDC
516.0496	5	1.7	GAFab	446	GAFab	449	EDC
713.8801	8	11	GAFab	150	GAFab	179	EDC
738.3687	4	5.4	GAFab	289	GAFab	305	EDC

Crosslinking conditions were followed as described in Fig. 3. Cross-linked peptides were identified following chemical cross-linking of GAFab pre-incubated with Pγ and cGMP and analyzed as described in *Methods*. Abbreviations are defined in the legend to Table S1.

Table S5. Inter-molecular cross-links identified for the Pγ-liganded state of PDE6C GAFab.

m/z	z	ppm	pep1	aa1	pep2	aa2	crosslinker
676.1063	4	-0.67	Pγ	29	GAFab	171	BS3
663.1042	4	-1.5	Pγ	23	GAFab	171	BS3
682.6824	3	-0.22	Pγ	29	GAFab	374	BS3
665.3475	3	0.5	Pγ	23	GAFab	374	BS3
449.0375	4	1.3	Pγ	43	GAFab	396	BS3
797.4662	2	0.042	Pγ	43	GAFab	319	BS3
378.975	4	-0.18	Pγ	43	GAFab	409	BS3
378.9749	4	-0.44	Pγ	42	GAFab	409	BS3
863.9749	2	0.63	Pγ	46	GAFab	319	BS3
573.6633	3	1.5	Pγ	39	GAFab	319	BS3
493.2857	4	-0.62	Pγ	39	GAFab	263	BS3
610.3389	2	-0.79	Pγ	43	GAFab	441	BS3
451.567	3	-1	Pγ	46	GAFab	441	BS3
655.366	3	-0.86	Pγ	29	GAFab	122	BS3
473.226	3	8.4	Pγ	27	GAFab	78	BS3
421.97	4	0.042	Pγ	23	GAFab	368	Sulfo-SDA
842.9329	2	0.25	Pγ	23	GAFab	369	Sulfo-SDA
475.7602	4	-2.1	Pγ	49	GAFab	263	Sulfo-SDA

Crosslinking conditions were followed as described in Fig. 3. Inter-molecular cross-linked peptides were identified following chemical cross-linking of GAFab pre-incubated with Pγ and analyzed as described in *Methods*. Abbreviations are defined in the legend to Table S1.

Table S6. Parameters for MD simulations

#	Atoms	Water	Length	Runs	Box size
X-ray	113990	33856	500 ns	3	87 Å × 131 Å × 107 Å
apo state	104728	30533	360 ns	3	88 Å × 120 Å × 107 Å
cGMP bound	104792	30531	360 ns	3	88 Å × 120 Å × 107 Å

Details of MD simulations on three different systems are highlighted including the numbers of total and water atoms in each simulation, the length of each trajectory (3 independent simulations for each system) and the dimensions of each simulation domain.

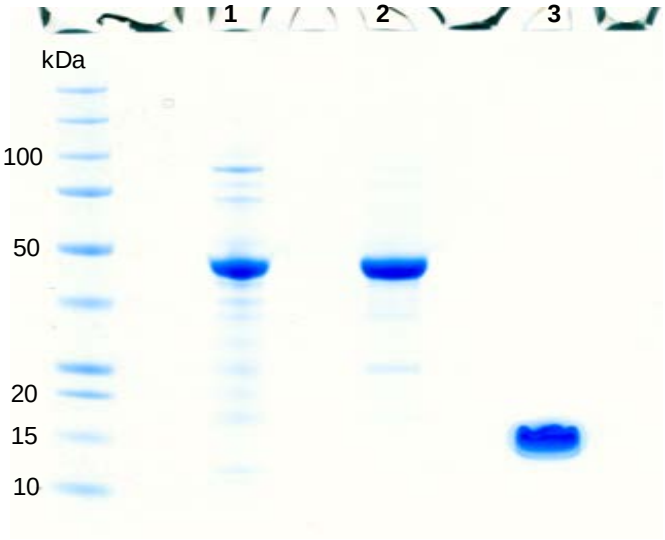

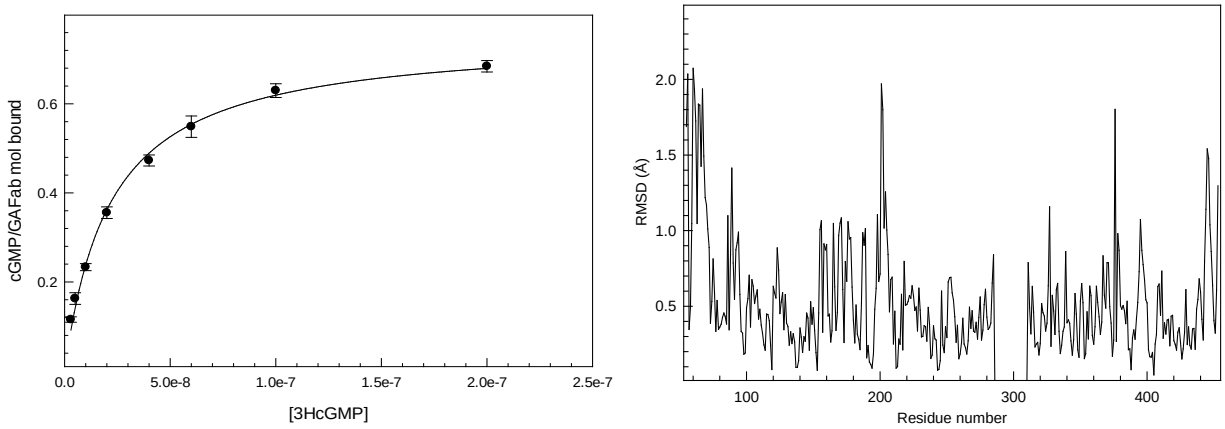

Fig S1. Purification, cGMP binding properties, and initial characterization of structural asymmetry of chain A and chain B of the x-ray structure. A. SDS-PAGE of purified, recombinant chicken cone PDE6 GAFab (PDE6C, residues 42-458) and chicken cone Pγ1-58. Lane 1, affinity-purified GAFab; Lane 2, gel filtration-purified GAFab; Lane 3, HPLC-purified Pγ1-58. **B.** Binding curve of 1.5 nM GAFab incubated with increasing concentrations of [3H]cGMP; the solid line represents fitting the data to a hyperbolic curve, with a K_D = 20 nM. **C**. RMSD analysis of chain A versus chain B of the chicken cone PDE6 GAFab x-ray structure; average RMSD value was 0.74 Å.

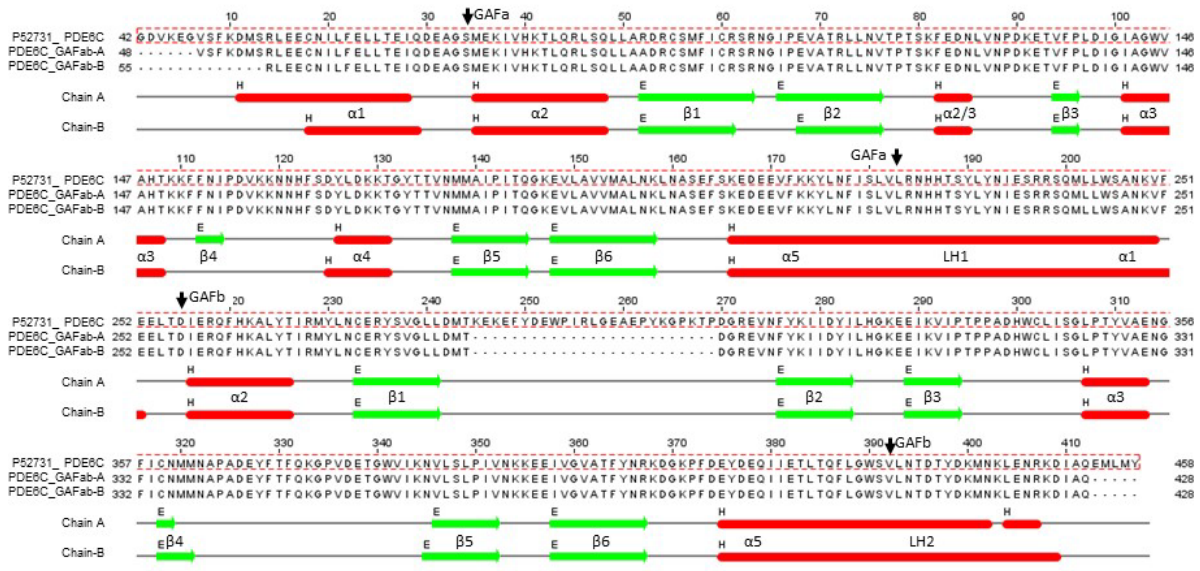

Fig. S2. Structural alignment of cone PDE6C regulatory domains. The chicken cone PDE6 amino acid sequence (PDE6C_CHICK, P52731) was aligned with the two subunits of the crystal structure (Fig. 2A) with secondary structure elements highlighted in red (α-helix) or green (β-strand). The boundaries for the GAFa (residues 75-224) and GAFb (residues 256-433) domains (black arrows) are defined according to their Pfam (PF01590) entry.

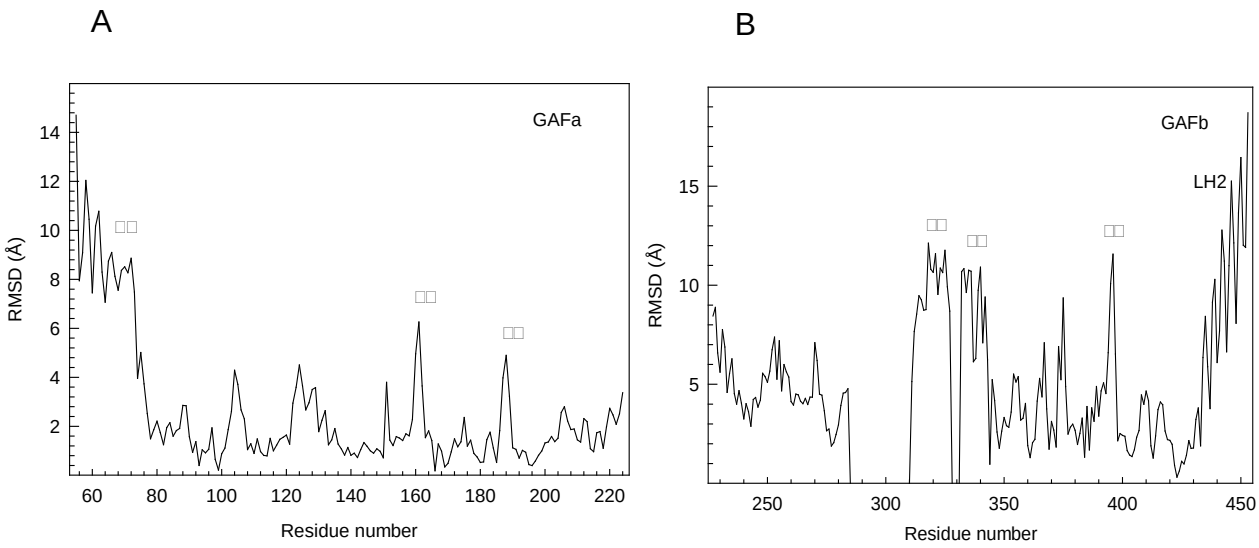

Fig. S3. Structural comparison of the GAF domains of rod and cone PDE6. A. The GAFa domain (residues 55-224 of the chicken cone sequence and the corresponding residues (59-228) of the bovine rod β-subunit {Irwin, 2019 #7890}) were aligned, and the RMSD values for each residue were determined. The overall average RMSD = ?? Å, and omitting the LH1 and LH2 regions resulted in an average RMSD = ?? Å. **B.** Comparative RMSD analysis of the GAFb domain of chicken cone (residues 225-453) with the bovine rod β-subunit (residues 229-457). The overall average RMSD = ?? Å, and omitting the LH1 and LH2 regions resulted in an average RMSD = ?? Å.

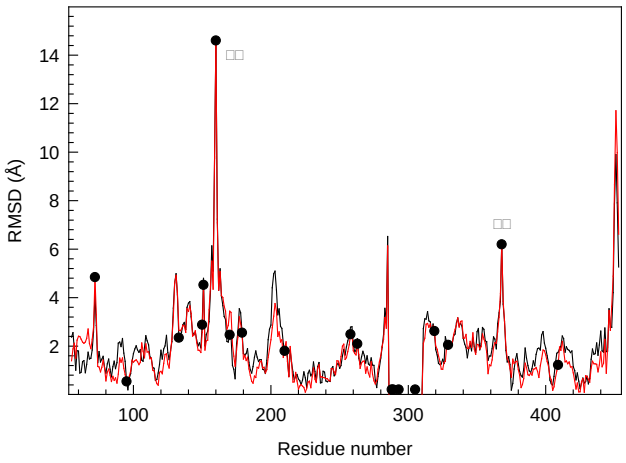

Fig. S4. RMSD analysis of the chicken cone GAFab x-ray structure versus the cross link-refined apo GAFab structure. The black and red lines represent RMSD values for A and B subunits of GAFab, respectively. Black circles identify intra-molecular crosslinked residues of GAFab. Note that the gap between residues 285 and 311 reflect the unresolved loop in the x-ray structure.

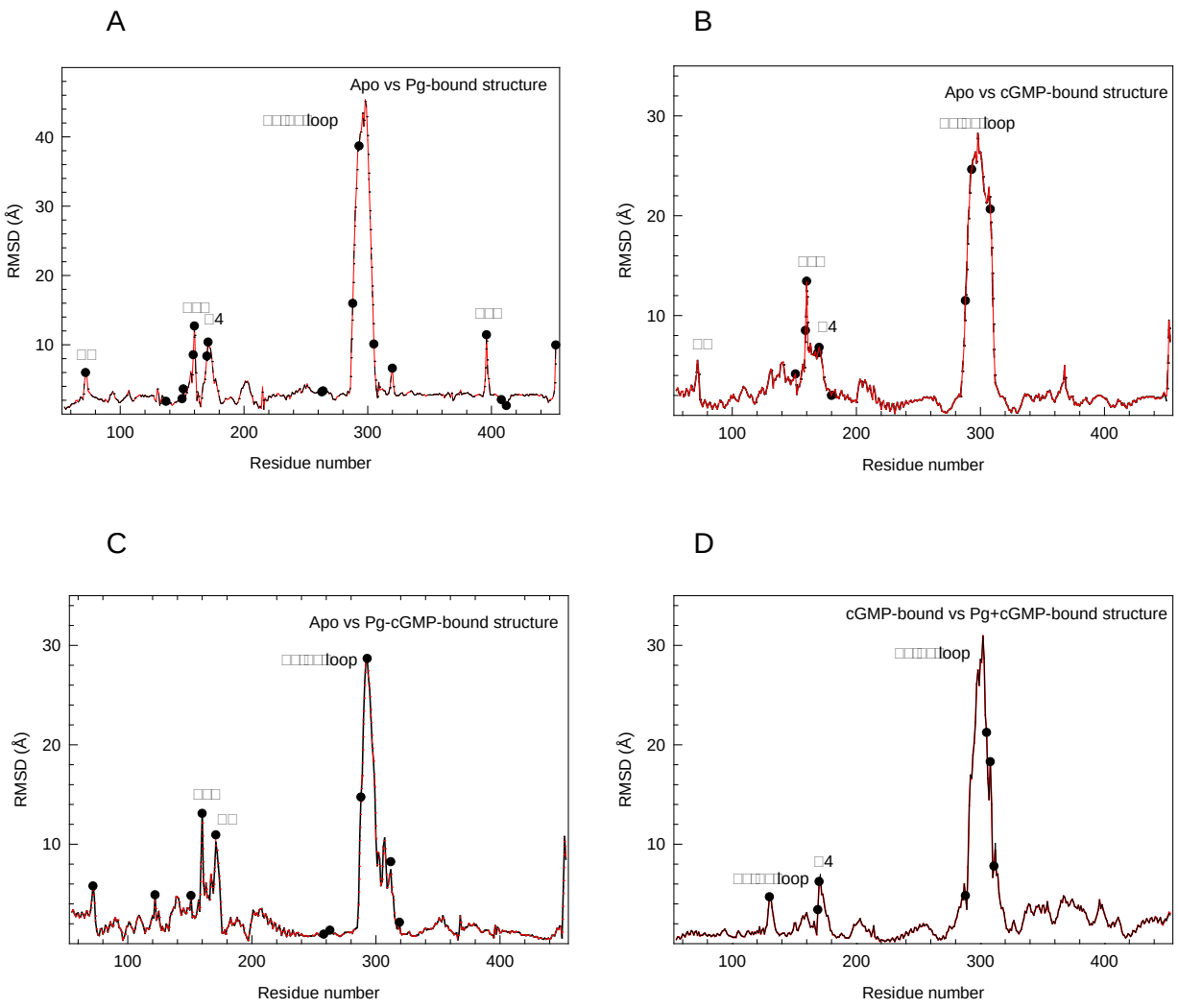

Fig. S5. RMSD plots for various liganded states of GAFab. RMSD per residue was calculated after aligning the apo GAFab structure with other liganded states. **A.** apo state versus Pγ1-58 bound to GAFab. **B.** apo state versus cGMP bound to GAFab. **C.** apo state versus Pγ1-58 plus cGMP bound to GAFab. **D**. RMSD per residue analysis between the Pγ-bound and Pγ- plus cGMP-bound GAFab. The black and red lines represent RMSD values for A and B subunits of GAFAB, respectively. Black circles represent intra-molecular crosslinked residues identified for each liganded state.

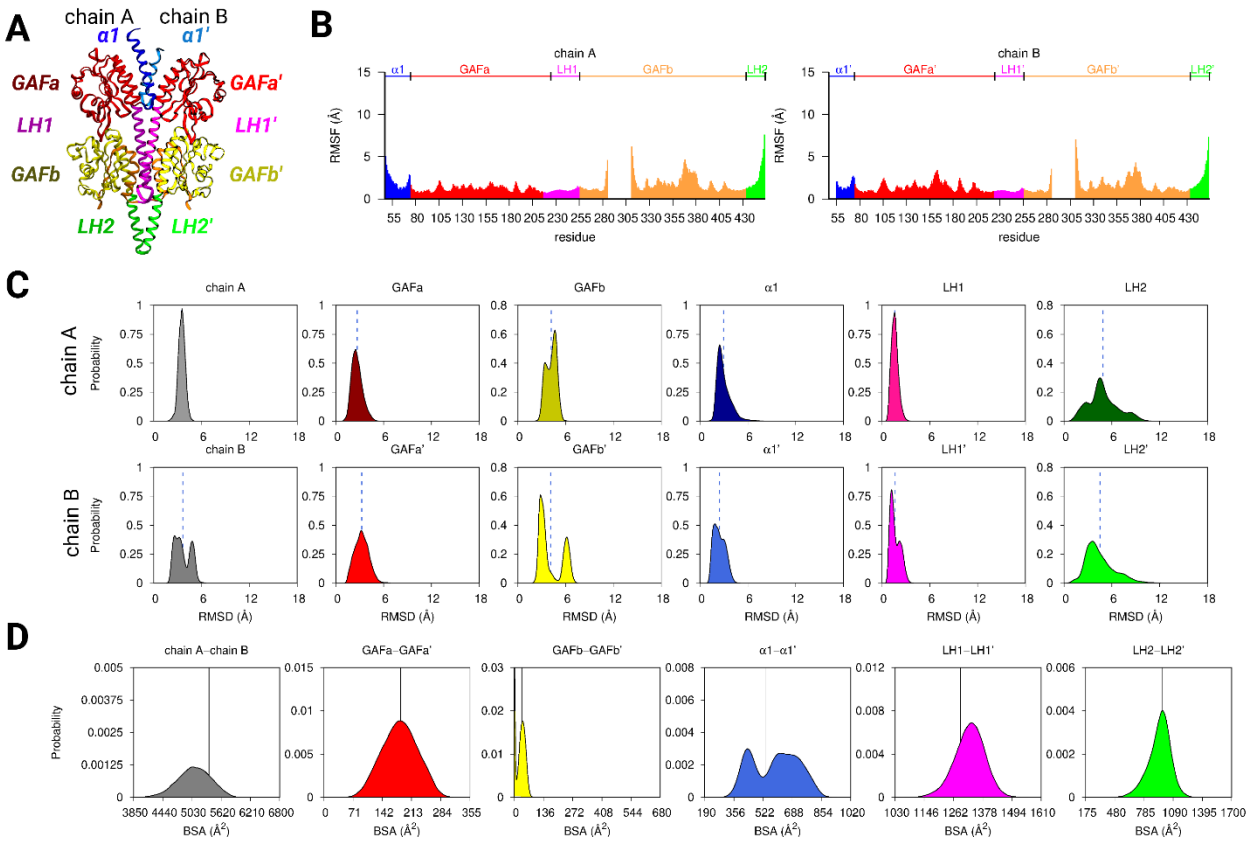

Fig. S6. Dynamics and stability of the crystal structure of the PDE6 GAFab homodimer as characterized by various conformational metrics. (A) Cartoon representation of the x-ray structure with color scheme for the subdomains characterized in panels B-D. (B) Root mean squared fluctutation (RMSF) per residue for each subunit, color-coded to correspond with the representation in panel A; (C) the probability distributions of the root mean squared deviation (RMSD) for individual domains of each subunit; (D) the distributions of the buried surface area (BSA) between various domains of the homodimer. Vertical lines marked on distributions correspond to mean values of the RMSD data from simulations (panel C) and the BSA values (panel D) observed in the crystal structure.

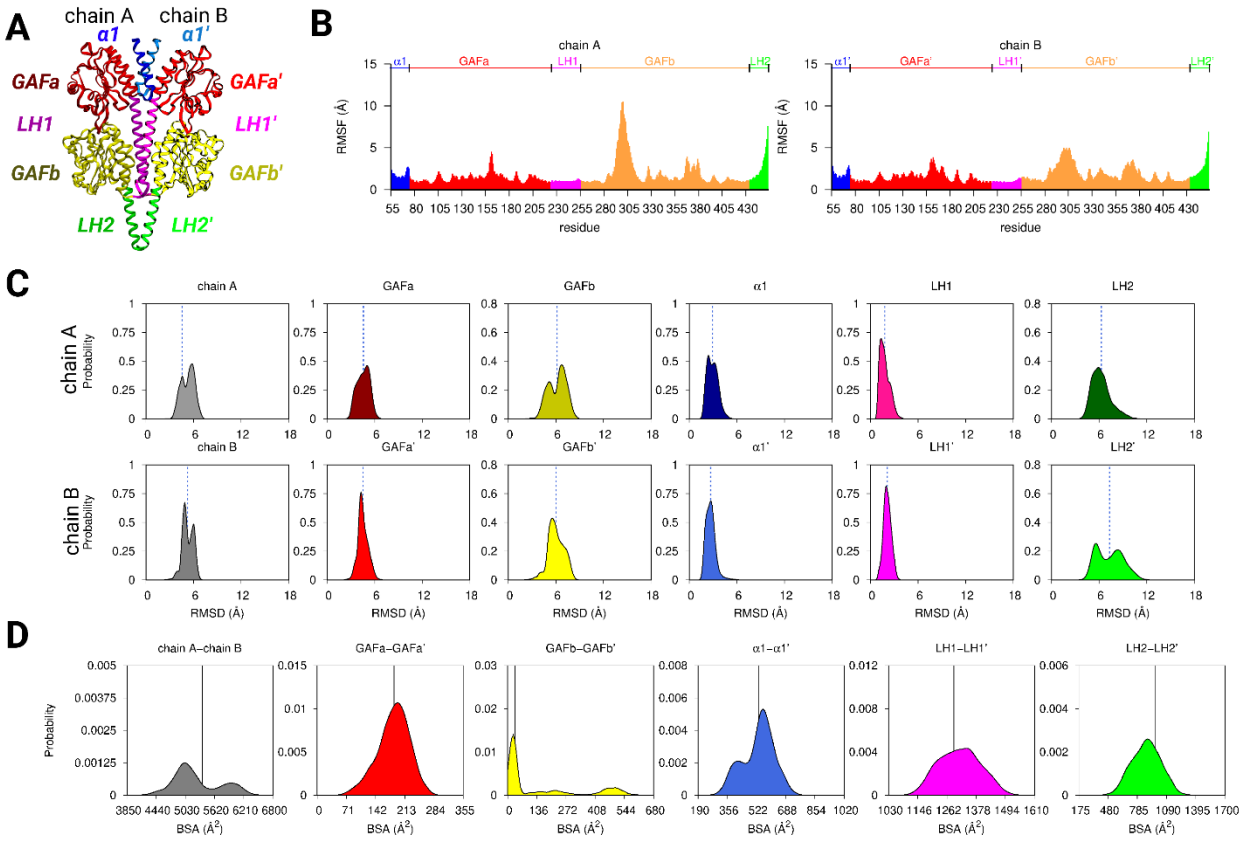

Fig. S7. Conformational metrics highlighting dynamics of the apo state of the PDE6 GAFab homodimer. For the apo-state of PDE6 (A), data similar to Fig. S6 are highlighted in panels B-D.

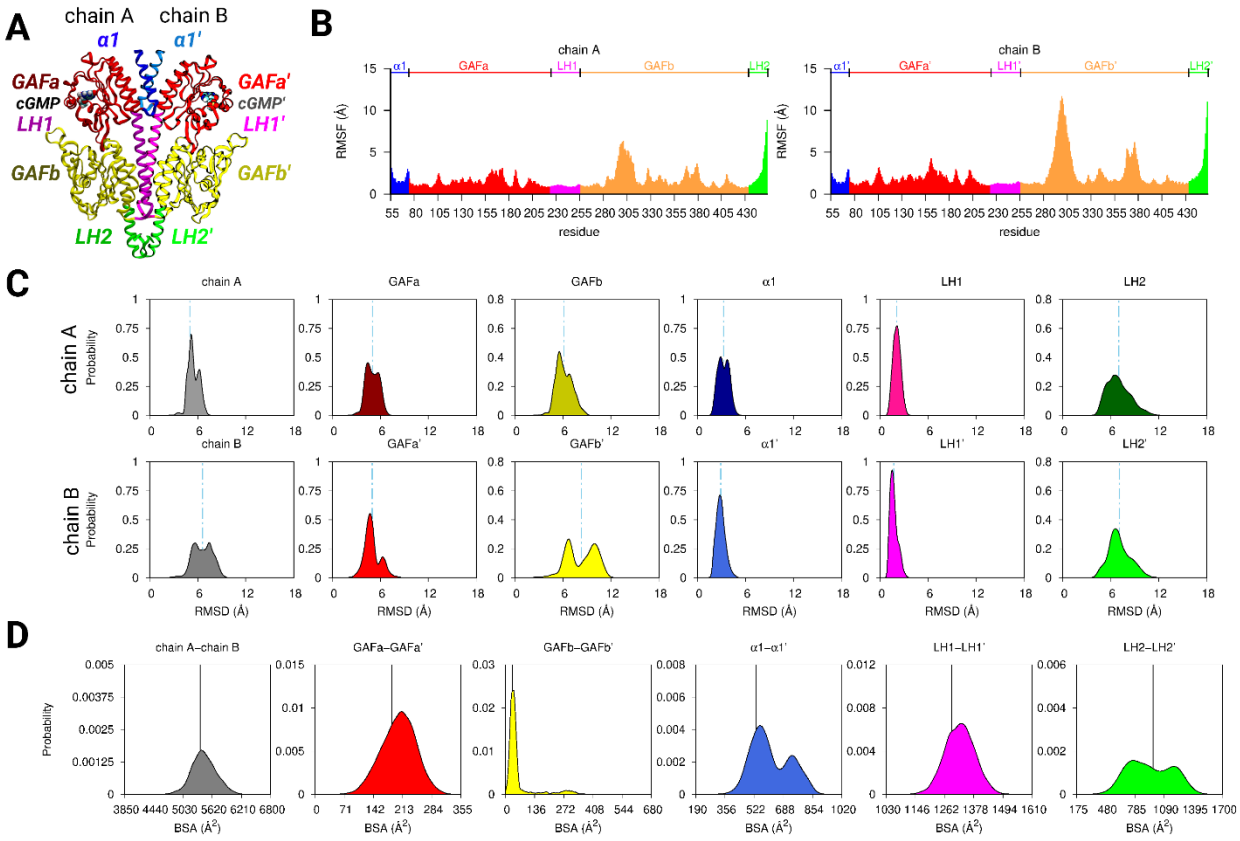

Fig. S8. Conformational metrics highlighting the dynamics of the cGMP-bound state of the PDE6 GAFab homodimer. For the cGMP-bound state of PDE6 (A), data similar to Fig. S6 are highlighted in panels B-D.